Journal of Volcanology and Geothermal Research 446 (2024) 107997

Contents lists available at ScienceDirect

Journal of Volcanology and Geothermal Research

journal homepage: www.journals.elsevier.com/journal-of-volcanology-and-geothermal-research

New evidence of the Green Tuff deposits and post-caldera, recent explosive volcanic activity at Pantelleria volcano (Sicily Channel, Italy) recorded in near-vent marine areas

C. Romagnoli [a,b,*], C. Giglio [a], A.M. Conte [b], A. Cloke-Hayes [c], M. Garcia [d], G. Gasparotto [a], S. Benetti [e]

[a] Dipartimento di Scienze Biologiche, Geologiche ed Ambientali, Università di Bologna, Piazza di Porta S. Donato 1, 40126 Bologna, Italy
[b] Consiglio Nazionale delle Ricerche - Istituto di Geologia Ambientale e Geoingegneria c/o Dipartimento di Scienze della Terra, Sapienza Università, P.le A. Moro, 500185 Roma, Italy
[c] Department of Geography, Mary Immaculate College, South Circular Rd, Limerick V94 VN26, Ireland
[d] Cadiz Oceanographic Center (IEO-CSIC), Cadiz 11006, Spain
[e] School of Geography and Environmental Science, University of Ulster, Cromore Road, Coleraine BT52 1WR, Ireland

ARTICLE INFO

Keywords:
Mediterranean tephrochronology
Stratigraphic marker
Marine sediments
Tephra preservation
Sicily Channel
Pantelleria

ABSTRACT

The record of the explosive activity of Pantelleria volcano is well documented by several distal tephra collected in various areas in and around the Mediterranean, while few tephrochronological studies exist on proximal marine areas. In this paper, we investigate three selected coring sites from the northern shoulder of the Pantelleria graben, about 15–30 km from the island, in near-vent position with respect to that volcanic source. Our multiproxy analyses revealed nine tephra layers, totally composed of juvenile materials, mostly ash and pumice fragments, as well as a coarse-grained tephra deposit at the bottom of one of the cores. The major element composition of glass shards indicates a very homogeneous geochemical composition for the tephra layers, suggesting their primary origin. Using litho-stratigraphic and paleoenvironmental proxies, we associated the tephra layers to the latest (<~13.7 ka) explosive activity of Pantelleria. The coarse-grained deposit, instead, due to its distinctive composition is considered to represent the near-vent, marine equivalent of the distal Y-6 tephra layer, related to the ~45 ka old co-ignimbrite fallout deposit of the Green Tuff event. The geochemical characterization of such deposit, mostly rhyolitic and partly trachytic, appears to enlarge the bimodal composition recorded in other distal tephra (Y-6) reported in the literature, highlighting the potential of near-vent record in providing additional information on the eruptive history.

1. Introduction

The record of volcanic activity in marine sediments represents a fundamental archive for the reconstruction of the eruptive history and style of active volcanoes, as original deposits may be best-preserved in the marine environment comparative to those on land. Over the last decades, marine tephra studies have allowed to significantly improve the reconstruction of the explosive activity of Mediterranean volcanoes (e.g. Keller et al., 1978; Paterne et al., 1986, 1988, 2008; Margari et al., 2007; Caron et al., 2010; Insinga et al., 2014; Tomlinson et al., 2015; D'Antonio et al., 2016; Wulf et al., 2018; Giaccio et al., 2019; Friedrichs et al., 2020; Vakhrameeva et al., 2021; Monaco et al., 2022), with important outcomes in terms of recurrence estimates of high-energy events and related potential hazard. In addition, the identification of tephra layers in marine and lacustrine sediments has supplied a significant stratigraphic and chronological support to paleo-climatic, paleo-oceanographic and archaeological investigations in the Mediterranean basin (Sulpizio et al., 2008; Caron et al., 2010, 2012; Zanchetta et al., 2018; Giaccio et al., 2012, 2019). The value of tephra as a correlation tool is due to the fact that primary marine ash-layers can be considered as instantaneous geologic events, providing good chronostratigraphic markers for deep-sea sediments (Paterne et al., 1988).

The Island of Pantelleria is the top of a large composite Quaternary volcano belonging to the magmatic district of the Sicily Channel in the central Mediterranean Sea (Fig. 1). According to Civile et al. (2010), this area represents an example of intraplate "passive" rift, where volcanism

* Corresponding author at: Dipartimento di Scienze Biologiche, Geologiche ed Ambientali, Università di Bologna, Piazza di Porta S. Donato 1, 40126 Bologna, Italy.
E-mail address: claudia.romagnoli@unibo.it (C. Romagnoli).

https://doi.org/10.1016/j.jvolgeores.2023.107997
Received 14 June 2023; Received in revised form 22 December 2023; Accepted 27 December 2023
Available online 2 January 2024

is a consequence of tensional stresses on the lithosphere due to the regional stress field in an anorogenic setting. The island is the type locality for "pantellerite", an iron-rich peralkaline rhyolite (Förstner, 1881). The volcanic activity at Pantelleria is characterized by a bimodal association of alkaline basaltic magma and peralkaline evolved magma products, the latter associated to explosive activity that produced large volumes of ignimbrites and pyroclastites (Villari, 1974; Cornette et al., 1983; Civetta et al., 1984; Mahood and Hildreth, 1986; Orsi et al., 1991). An impressive ignimbritic episode at ~45 ka BP caused the emplacement of a pyroclastic sheet blanketing the whole island, the so-called Green Tuff (hereafter GT; Mahood and Hildreth, 1986; Civetta et al., 1988; Rotolo et al., 2013, 2021). This eruption represents the last high (est) magnitude eruption on the island and is usually related to a well-defined distal tephra layer (Y-6) recorded throughout the Central and Eastern Mediterranean, that represents a geochemically unique and regionally extensive key-horizon (Keller et al., 1978; Mahood and Hildreth, 1986; Paterne et al., 1988; Narcisi and Vezzoli, 1999; Margari et al., 2007; Vogel et al., 2010; Sulpizio et al., 2010; Scaillet et al., 2013; Tamburrino et al., 2012; Zanchetta et al., 2018; Rotolo et al., 2021).

The Eurofleets2-funded PANTHER (*PANTelleria High-Energy ERuptions from marine studies*) project aimed to broaden the knowledge on the eruptive activity of Pantelleria through the marine record using geophysical and sedimentological data. This paper presents key results from three cores collected in marine areas in the proximity of the island (about 15–30 km to the NE; cores PAN05, PAN06 and PAN07; Fig. 1b), providing evidence of the latest (<13.7 ka) explosive volcanic activity on the island, but also of the possible primary marine equivalent of the GT deposit/tephra layer. The latter is here sampled in a near-vent area, providing new insights with respect to more distal equivalents of the same eruptive event largely reported in literature (see references above).

2. Geological and oceanographic setting of Pantelleria volcano

Located in the central Mediterranean Sea, the Sicily Channel belongs

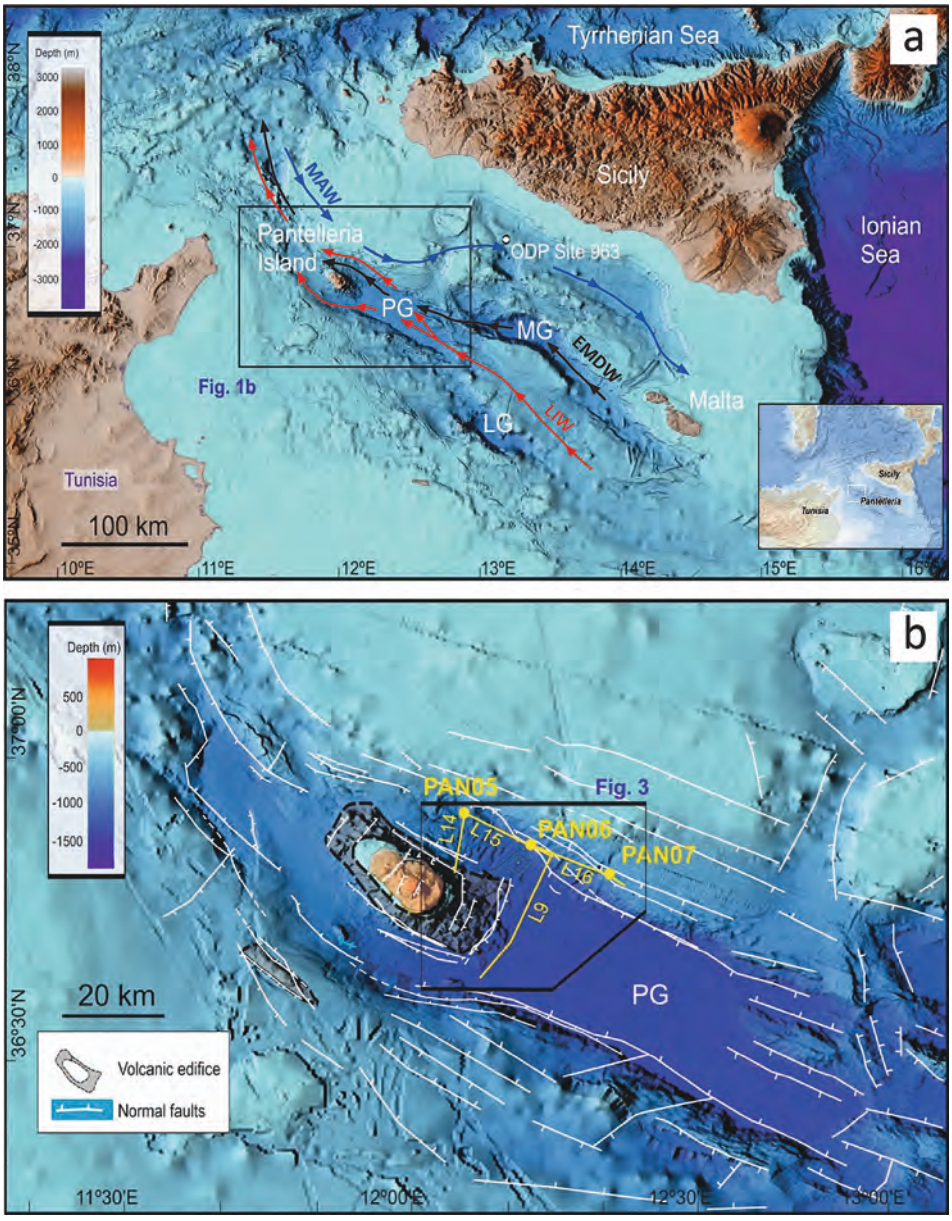

Fig. 1. (a) Location of Pantelleria Island in the Sicily Channel. PG: Pantelleria Graben, MG: Malta Graben, LG: Linosa Graben. The main water masses in the Sicily Channel (from Gauchery et al., 2021) are indicated: MAW, Modified Atlantic Water; LIW, Levantine Intermediate Water, and EMDW Eastern Mediterranean Deep Water; (b) structural sketch map (from Civile et al., 2010, modified), with location of the studied cores.

to the northern part of the African continental plate, i.e. the Pelagian Block (Burollet et al., 1978). During the Neogene-Quaternary it has been affected by processes of continental rifting and crustal thinning that produced the Pantelleria, Malta and Linosa tectonic depressions (grabens), with water depths ranging from 1300 to >1700 m (Fig. 1a), and favoured magma rising (Colantoni, 1975; Calanchi et al., 1989).

Pantelleria Island (area of ~83 km^2) represents the small (<20% of the whole extension) emergent tip of an underwater, NW-SE elongated volcanic edifice rising from a maximum depth of ~1300 m up to 836 m above sea level in the north-western portion of the Pantelleria basin (Bosman et al., 2011; Fig.1b). This ~90 km long and 30–40 km wide basin deepens gently, from ~1280 m water depth (mwd) at the base of Pantelleria island to 1330 mwd in the south-eastern area. The basin is bounded by NW–SE trending, sub-vertical conjugate normal faults (Fig. 1b) and partially filled by lower Pliocene–Quaternary deposits reaching a thickness over 1000 m (Civile et al., 2010). Magmatic activity in the basin is progressively more diffuse and shallow moving from SE to NW, up to emerge in Pantelleria Island (Civile et al., 2010).

The known activity of the Pantelleria subaerial volcano is older than 320 ka (Mahood and Hildreth, 1986). Related volcanic products on the island are mainly represented by acidic rocks, ranging from rhyolites (pantellerites) to trachytes, and minor transitional basalts, emitted in a wide range of eruptive styles (Villari, 1974; Cornette et al., 1983; Mahood and Hildreth, 1983, 1986; Civetta et al., 1988; Orsi et al., 1991). The focus of the sub-aerial volcanic activity apparently propagated north-westward with time: the oldest products outcropping on the island, pantelleritic and trachytic lavas (239–325 ka old, Mahood and Hildreth, 1986) are only exposed into cliff sections along the S–SE coast of the island, while the recent basaltic rocks are exposed in the north-western sector (Fig. 2). The volcanic activity of Pantelleria was mainly explosive and produced large volumes of ignimbrites and pyroclastites associated with the development, in the south-eastern portion of the island (Fig. 2) of a large caldera complex, whose collapse dates back to 140–146 ka and 45–50 ka (La Vecchia Caldera and Cinque Denti Caldera, respectively; Cornette et al., 1983; Mahood and Hildreth, 1986; Speranza et al., 2012; Rotolo et al., 2021). The latter event corresponds to the emplacement of the Green Tuff, consisting of a complex sequence of surge and air fall deposits, and by welded ignimbrite (Mahood and Hildreth, 1983, 1986; Civetta et al., 1988; Di Genova et al., 2013). The terrestrial volume of the deposit was estimated at 0.49–0.60 km^3 (Wolff and Wright, 1981; Mahood and Hildreth, 1983), recently re-evaluated at 0.28 km^3 (Jordan et al., 2018). The dominant composition of the GT appears to be pantellerite, and a less evolved trachyte magma is represented in the pyroclastic unit emplaced at the top of the GT sequence (Lanzo et al., 2013; Scaillet et al., 2013; Cinquegrani et al., 2022). The most recent high-precision $^{40}Ar/^{39}Ar$ dating constrains the GT eruption at 45.5 ± 1.0 ka (Zanchetta et al., 2018) or 43.9 ± 0.5 ka for the top trachytic member (Cinquegrani et al., 2022). Williams (2010)

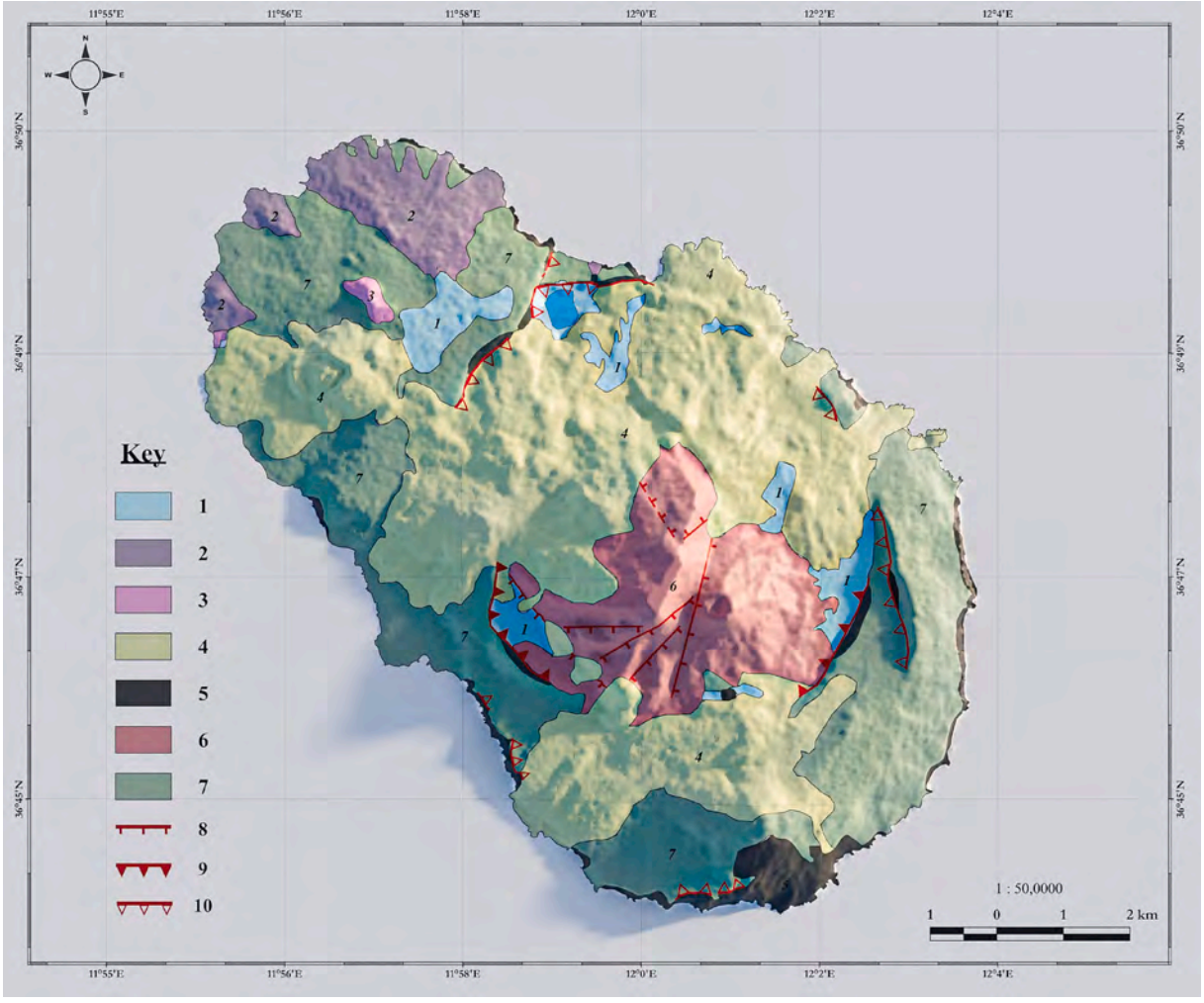

Fig. 2. Simplified geological map on Pantelleria DTM, with indication of the pre-, syn and post-GT units and of main volcano-tectonic lineaments (from Scaillet et al., 2013; modified after Rotolo et al., 2013). Legend: 1-Alluvium and fill; 2-Post-Green Tuff basalts; 3-Pre-Green Tuff basalts; 4-Post-Green Tuff pantelleritic pumice falls and lava flows; 5-Pre-Green Tuff pantellerites; 6-Trachyte lavas; 7-Green Tuff; 8-Faults; 9-Cinque Denti caldera rim; 10-La Vecchia caldera rim. (For interpretation of the references to colour in this figure legend, the reader is referred to the web version of this article.)

interpreted the GT deposit as resulting from a single eruption producing a sustained pyroclastic density current, and showed that it radially flowed from the source, locally breaching the caldera rim and overtopping topographic highs, then flowing unrestricted to the sea. An 8 m-thick, coarse, lapilli-tuff deposit has been recorded in a 30 m-long core from the Pantelleria Graben, over 50 km from the coastline to the SE, and interpreted to represent the direct deposition from the Green Tuff pyroclastic density current in the sea, overlaid by volcaniclastic turbidity currents (Anastasakis and Pe-Piper, 2006).

While the pre-50 ka volcanic history of Pantelleria cannot be reconstructed with detail due to the paucity and the scattering of related outcrops and due to the blanketing of the whole island by the GT deposits (Fig. 2), the post-caldera eruptive stage is relatively well known. It includes >50 low-energy strombolian-type eruptions of pantellerite pumice and lava flows/domes emitted by several centres (Rotolo et al., 2013, 2021) and has been subdivided into six eruptive cycles (the first one corresponds to the GT event), each one beginning with a mildly explosive phase, recorded by pantelleritic pumice fall deposits, followed by effusive activity, and separated by quiescence periods (Cornette et al., 1983; Mahood and Hildreth, 1983, 1986; Civetta et al., 1988; Orsi et al., 1991; Rotolo et al., 2013; Di Genova et al., 2013). However, recent chronologic studies of the intra-caldera eruptive activity (Scaillet et al., 2011) do not support the five cycle subdivision of the post-GT activity, and suggest that this later activity was characterized by short eruptive periods, punctuated by repose intervals of some millennia, having decreasing duration towards the present (Speranza et al., 2010).

The most recent eruption of Pantelleria was submarine and occurred in 1891 about 5 km NW of the western coast of the island. This eruption was unusual as it produced floating basaltic lava bombs Foerstner (1891); Riccò, 1892; Washington, 1909). Conte et al. (2014) and Kelly et al. (2014) have interpreted, as the possible 1891 vent, a small cone rising ~90 m from 350 m water depth, within a newly discovered submarine volcanic field located 4 km northwest of the Pantelleria harbour.

2.1. Pantelleria tephra

The widespread findings of tephra layers with peralkaline signature, related to the volcanism of Pantelleria, in both marine and lacustrine successions in the central and eastern Mediterranean area demonstrate the wide dispersion of the deposits generated during the explosive events, which reached distances of up to 1200 km away from their source along a main NE-ward dispersal axis (Wolff and Wright, 1981; Narcisi and Vezzoli, 1999; Margari et al., 2007; Paterne et al., 2008; Caron et al., 2010; Vogel et al., 2010; Tamburrino et al., 2012; Damaschke et al., 2013; Insinga et al., 2014; D'Antonio et al., 2016; Zanchetta et al., 2018). Among the distal deposits, the most widespread marker horizon has been correlated with the GT eruption, which is believed to have generated the Y-6 tephra in marine sequences in the Ionian Sea and Sicily Channel (Keller et al., 1978; Narcisi and Vezzoli, 1999; Tamburrino et al., 2012), in lacustrine records in Greece and Albania (Margari et al., 2007; Vogel et al., 2010) and in the Marsili Basin, southern Tyrrhenian Sea (Tamburrino et al., 2016). Tephra ODP1 sampled in the Sicily Channel (Site 963 in Fig. 1a, Tamburrino et al., 2012) has been considered up to now as the most proximal facies of the Y-6 layer sampled in the marine setting. The wide dispersal of the Y-6 distal equivalent of the GT is diagnostic of a large-magnitude eruption associated with caldera-collapse and emission of a Plinian convective plume, similar in importance to the Minoan eruption in the Aegean Sea (Scaillet et al., 2013). Tephra Y-6 has been correlated by Orsi and Sheridan (1984) with the basal part of the GT formation, which represents the Plinian fall member. More recently, the terminal, volumetrically dominant, co-ignimbrite ash-flow units have been considered the most likely source for the distal tephra Y-6 (Scaillet et al., 2013).

From a chemical point of view, the GT proximal deposits have a continuous trend from pantellerites at the base to comenditic trachytes at the top (Mahood and Hildreth, 1986; Civetta et al., 1988; White et al., 2009; Vogel et al., 2010). A similar zoning in chemical composition is found in other proximal and distal GT marine equivalents, while in some other deposits only the more differentiated terms were recovered (e.g., Tamburrino et al., 2012; Margari et al., 2007; Tamburrino et al., 2016, respectively).

2.2. Oceanographic setting

The Strait of Sicily connects the western and eastern sub-basins of the Mediterranean and is the seat of water exchange, basically driven by anti-estuarine thermohaline circulation. The water masses involved in this exchange are: an eastward directed surface layer (MAW, Modified Atlantic Water) that flows in the upper 100–200 m of water column, while a saltier layer (LIW, Levantine Intermediate Water) and a colder and denser bottom current (EMDW, Eastern Mediterranean Deep Water) flow westward at 200–700 mwd and >700 mwd, respectively (Astraldi et al., 2002; Fig. 1a). These latter water masses interact with the complex seabed morphology of the Sicily Channel (Gauchery et al., 2021) and, in the Pantelleria Graben, are considered to split into two branches at both sides of the Pantelleria volcanic edifice. Evidence of contouritic depositional and erosive features are recognized on the seabed to the N and SW of the island (Martorelli et al., 2011).

3. Data and analytical methods

An expedition on board the Italian National Research Council's RV *Minerva Uno* was carried out from 6 to 11 August 2016 in the framework of the PANTHER Project financed by Eurofleets 2. Three cores were collected on the northern shoulder of the Pantelleria graben, to the north-east of the island (PAN05, PAN06 and PAN07 in Fig. 1b and Table 1) with a 6-m barrel gravity corer.

To select the coring sites, very high-resolution profiles were acquired using a Chirp Swan Pro 2.02 system, working with a pulse length of 10 ms and a trigger rate between 0.25 and 2 s varying with depth. Maximum signal penetration was around 80 m with resolutions in the order of 1 m. Chirp profiles recorded in XTF format were converted into SEGY files using the SeisPhro LCL 2.0 software (Gasperini and Stanghellini, 2009) and displayed and analysed using the HIS Kingdom Suite. Coring sites were selected where relatively undisturbed sequences could be identified.

After recovery, cores were cut into 1 m sections, and continuously stored at 4 °C. Prior to splitting, cores were X-rayed at the School of Radiology at Ulster University using a CARESTREAM DRX-Evolution System. The X-radiographs were used to identify sedimentary structures not visible to the naked eye, including micro-scale bioturbation, fine-scale laminations and shear surfaces. Gamma ray density, magnetic susceptibility and P-wave velocity measurements were also obtained on the whole cores every 1–2 cm intervals using a GEOTEK Multi Sensor Core Logger (MSCL) at the Irish Sediment Core Facility at Maynooth University. The measurement of these physical properties allows detecting of lithological and compaction information. Cores were split and described at the Tullow Oil Core Handling Facility at University College Dublin (Ireland). Lithofacies were identified based on the combination of visual analysis (i.e., colour; structure; grain size), X-radiographs and MSCL physical properties.

Identification of planktonic foraminifera were performed on selected samples of cores PAN05 and PAN07 at Mary Immaculate College (Limerick, Ireland) to support stratigraphic interpretations inferred from

Table 1
Core location, depth and length. CC: core catcher.

Core	Lat (°N)	Long (°E)	Depth (m)	Recovery (m)
PAN05	36.9023	12.0921	746	5.44
PAN06	36.8495	12.2095	993	5.59
PAN07	36.8003	12.3472	668	5.29 + CC

radiocarbon dating and allow bio-stratigraphical correlation of cores and horizons across cores. Initially all samples were dried at ~40 °C to obtain a total sample weight. Each sample was then soaked in deionized water to allow the disaggregation of sediment before sieving through a 63 μm mesh. Dried samples were then sieved through a 150 μm mesh to obtain the larger fraction size from which planktonic foraminiferal census counts were obtained. Relative abundances are based on samples consisting of a minimum of 300 specimens. If necessary, larger samples were split into suitable aliquots using a sample microsplitter. Species identification is based on the taxonomic classification outlined by Hemleben et al. (1989). Sampling resolution varies between 10 and 20 cm therefore suggested calendar ages are approximate (Table 2 and Section 4.1.3). The observed faunal signals and associated ecozones are based on those identified by Sprovieri et al. (2003; Table A1 in the Appendix) from a nearby core in the Straits of Sicily (ODP Site 963, Fig. 1a).

Seven samples of micro- and macro-fossils were picked for radiometric analyses from selected core horizons of cores PAN05 and PAN07 for assessing the chronostratigraphic framework of the cores, including the calculation of sedimentation rates and of the ages of key tephra-rich layers. Only whole, unabraded mixed planktonic foraminifera specimens from >150 μm fraction and whole or almost whole bivalve shells were picked, indicating undisturbed deposition. Radiocarbon analyses were carried out at Beta Analytic Laboratories (Miami, Florida) and at the Keck Carbon Cycle AMS Facility at the University of California (Irvine, USA; UCIAMS). The conventional ^{14}C ages were calibrated with Calib 8.20 using the Marine20 calibration curve with a calculated ΔR for the region of −115.0 +/− 75 year (Stuiver et al., 2021). The ages are reported in the text as the rounded calibrated 2σ median results (Table 3 and Section 4.1.3).

Tephra-rich layers were identified in the cores by visual inspection and sampled during the core logging and description, on the basis of the abundance of volcanogenic material, of their primary setting in the sedimentary sequence, and through comparison with their magnetic properties (see Section 4.1.2).

Collected samples were washed in distilled water and dried in oven at 40°. Glass and pumice shards were hand-picked under a binocular microscope and subjected to morphological analyses. For major elements chemical analysis, 10–20 shards were mounted on epoxy resin beads and polished. Analyses on single pumice and glass grains were carried out with SEM-EDX (Philips 515b/EDAX DX4 at BiGeA Department, University of Bologna) and electron microprobe (EMPA) Cameca SX50–52, equipped with a five wavelengths dispersive spectrometer (WDS) at Istituto di Geologia Ambientale e Geoingegneria (CNR, Roma). Measuring conditions were 15 kV accelerating voltage, 2 nA beam current, 100 s counting time for SEM-EDX, and 15 kV accelerating voltage, 15 nA beam current, 10 s counting time (20 s for peaks) for EMPA. To minimize the well-known problem of Na-loss, a defocused electron beam of 15–20 μm was used and Na was counted first; for EDS the beam was scanned over an area of about 5*4 μm. ZAF correction was used for EDX, PAP routine (Pouchou and Pichoir, 1991) for matrix effects in EMPA. Standards used were for EDX: anorthoclase (Na, Al, Si), olivine (Mg, Fe), ilmenite (Ti, Mn), microcline (K), anorthite (Ca), scapolite (Cl), all from the Smithsonian Microbeam Standards collection (https://naturalhistory.si.edu/research/mineral-sciences/collections-overview/reference-materials/smithsonian-microbeam-standards); for EMPA: wollastonite (Si and Ca), corundum (Al), diopside (Mg), andradite (Fe), rutile (Ti), orthoclase (K), jadeite (Na), phlogopite (F), KCl (Cl), barite (S), and metals (Mn). The Ti content was corrected for the overlap of the Ti and Ba peaks. To evaluate the accuracy of the analyses, three international secondary standards (Kakanui augite, Icelandic Bir-1 and rhyolite RLS132 glasses from USGS) were measured prior to analyses. The mean precision was about 1% for SiO_2, 2% for Al_2O_3, 6% for K_2O, CaO and FeO, and 8–10% for the other elements. For EDX an account of the accuracy / precision can be found in Calanchi et al. (1994) and (1998).

About 20 analyses were performed on each shard; individual analyses with total oxide sums <94% were excluded. All the analyses were recalculated to 100% free of F + Cl + SO_3 (for EMPA), Cl (for EDX). The analytical data set (see file in ESM) was checked by comparing the results from both EMPA-WDS and EDX. Differences for major elements contents between the two analytical methods in samples with trachytic composition are <3%, except for Na_2O (about 10%, see file in ESM). In samples with rhyolitic (pantelleritic) composition, having a much wider data set (see ESM), differences in major elements between EMPA-WDS and EDX analytical data are <2%, except for in Al_2O_3 and FeO, which show differences in the order of 8.5 and 4.5%, respectively. However, these differences can be considered do not affect the comparability among the analysis and the results interpretation.

4. Results

4.1. Core setting and stratigraphy

4.1.1. Bathymetric and subseafloor setting

Sediment cores were retrieved from the NW-SE oriented escarpment that forms the northern margin of the Pantelleria Graben and connects the gently sloping seabed on top of the northern shoulder of the graben (depth over 650 mwd) with the basin floor (Fig. 1b). This margin is not straight, but it displays an articulated shape from SE to NW (Fig. 1b): in particular, it is formed by a narrow and steep slope (2.5–3 km wide and with gradients up to 25°) in the southern part of the Pantelleria Graben while, towards the NW, where sediment cores were retrieved, the slope is slightly recurved and overall less steep (12–18 km wide and <12° of

Table 2
Samples selected for biostratigraphical analyses and results for PAN05 and PAN07.

Core depth (cm)	Faunal signals	Ecozone	Approximate calendar age (cal BP)	Event
PAN05				
134	Reappearance of *Globorotalia truncatulinoides* (dominated by the dextral form).	3F (upper)	~5 k	Mid-Late Holocene
284–304	Peak frequencies (~52%) of *Globigerinoides ruber* (white).	4F (lower)	8.5 k–9.2 k	Unit S1a of Sapropel 1
324	Peak frequencies (~40%) of *Globorotalia inflata.*	5F	~10 k	Early Holocene
344–384	Increasing frequencies of *Turborotalia quinqueloba* and *G. inflata.* Decreasing frequencies of *G. ruber*.	6F	11.6 k–12.9 k	Younger Dryas
464–544	Faunal assemblage is dominated by *Globigerina bulloides*, *Neogloboquadrina incompta* and *T. quinqueloba*. Noted absence of *G. ruber* and *G. inflata*.	8F	14.7 k–22.8 k	Glacial Period
PAN07				
208–209	Faunal assemblage is dominated by *G. bulloides*, *G. inflata* and *G. ruber*. Minor species include *N. incompta* and *Globigerina glutinata*.	7F	13 k–14.7 k	Bølling-Allerød period
320–321	Faunal assemblage is dominated by *N. incompta*, *G. bulloides* and *G. ruber*. Minor species include *T. quinqueloba*, *Globorotalia scitula* and *G. glutinata*. There is a notable absence of *G. inflata*	8Fa	21.2 k–22.8 k	Glacial Period

Table 3
Samples submitted for radiocarbon dating and obtained age (dates in text are rounded to the nearest 10y as recommended by calibration results in Calib 8.20).

Core	Depth (cmbsf)	Material	Weight (mg)	Lab numb[a]	Conventional radiocarbon age in yrs BP	Calibrated 2σ age range in yrs BP (median probability)
PAN05	18–19	Foraminifera	9.8	Beta-490423	190 ± 30	1870 - Post 1950 CE
	205–206	Foraminifera	2.7	Beta-682492	6150 ± 30	6287–6729 (6507)
	255–256	Foraminifera	8.0	Beta-488477	7480 ± 30	7658–8081 (7870)
PAN07	195–196	Foraminifera	4.4	UCIAMS-225385	12,220 ± 220	13,147–14,427 (13731)
	320–321	Foraminifera	4.6	Beta-673897	18,810 ± 60	21,699–22,295 (22006)
	420–422	Foraminifera	8.8	Beta-497191	24,610 ± 90	27,711–28,399 (28022)
	484–487	Mixed bivalves	4.5	Beta-584020	29,720 ± 160	33,059–33,975 (33521)

[a] The first part of the lab number indicates the actual analytical laboratory (Beta for Beta Analytic Laboratories and UCIAMS for AMS laboratory at University of California USA).

gradient). The base of the slope shallows towards the NE, from about 1330 to <600 mwd. The Chirp profile L16 (Fig. 3) crossing the coring site PAN07, located at 668 mwd on the upper slope, shows parallel layered facies, with high lateral continuity of reflections and high acoustic amplitude that gradually decreases below about 60 ms (about 45 m considering a sound speed of 1500 m/s twt). Similarly, the seismic character in the coring site PAN05, located at 746 mwd, is stratified, and distinct layers bounded by high-acoustic amplitude reflections can be identified (profiles L14 and L15 in Fig. 3). In the coring site of PAN06, located in the lower slope at 993 mwd, a 40 m-thick upper layer with parallel-layered character, but medium acoustic amplitude and good lateral continuity, overlies a more acoustically transparent facies with some internal reflections (Fig. 3, line L15). Down along the slope and in the basin (lines L14 and L9 in Fig. 3), Chirp profiles show that the stratified upper sequence is variable in thickness and locally covers irregular, chaotic-transparent layers (possible mass transport deposits). However, the overall seismoacoustic setting suggests a relatively undisturbed recent sedimentation, especially in the PAN05 and PAN07 coring sites located in the upper slope.

4.1.2. *Litho-stratigraphy*

Lithological logs of the cores and facies interpretation are summarized in Fig. 4. The cores consist predominantly of muddy sediments, including clays and silty mud, punctuated by the occurrence of coarser-grained tephra layers. Four lithofacies were identified in the cores: 1) fine hemipelagite; 2) coarser, foraminifera-rich hemipelagite; 3) contourite; and 4) tephra layers. All three cores include the first three facies from bottom to top and can be roughly correlated based on sediment colour, grain size and sorting, degree of bioturbation and physical properties derived from the MSCL measurements. Tephra layers are found mostly within the upper, coarser hemipelagite (Fig. 4; here the tephra layers are named A, B and C simply based on their appearance in the core from the top towards the bottom. This labelling does not imply that the layers necessarily correlate among cores). The four lithofacies are described as follows:

(1) The bottom 1.5–2 m of all cores is a hemipelagite (cf. Stow and Piper, 1984) consisting of structureless clay, grey to olive grey in colour, only lightly bioturbated. Magnetic susceptibility values are always under 10 SI, density is <1.5 g/cc, and p-wave velocity always below 1660 m/s.

(2) Above this, another hemipelagic facies is richer in foraminifera and slightly coarser. This foraminifera-bearing sandy/silty mud layer is around 3–3.5 m thick, varies in colour from yellowish brown to olive grey and olive brown, and bioturbation is minor to moderate. Magnetic susceptibility is around 10 SI, p-wave velocity is always between 1650 and 1700 m/s and density around 1.4–1.6 g/cc.

(3) The top of all cores is a brown laminated silty mud, between 10 and 20 cm thick, interpreted as the result of contouritic reworking and

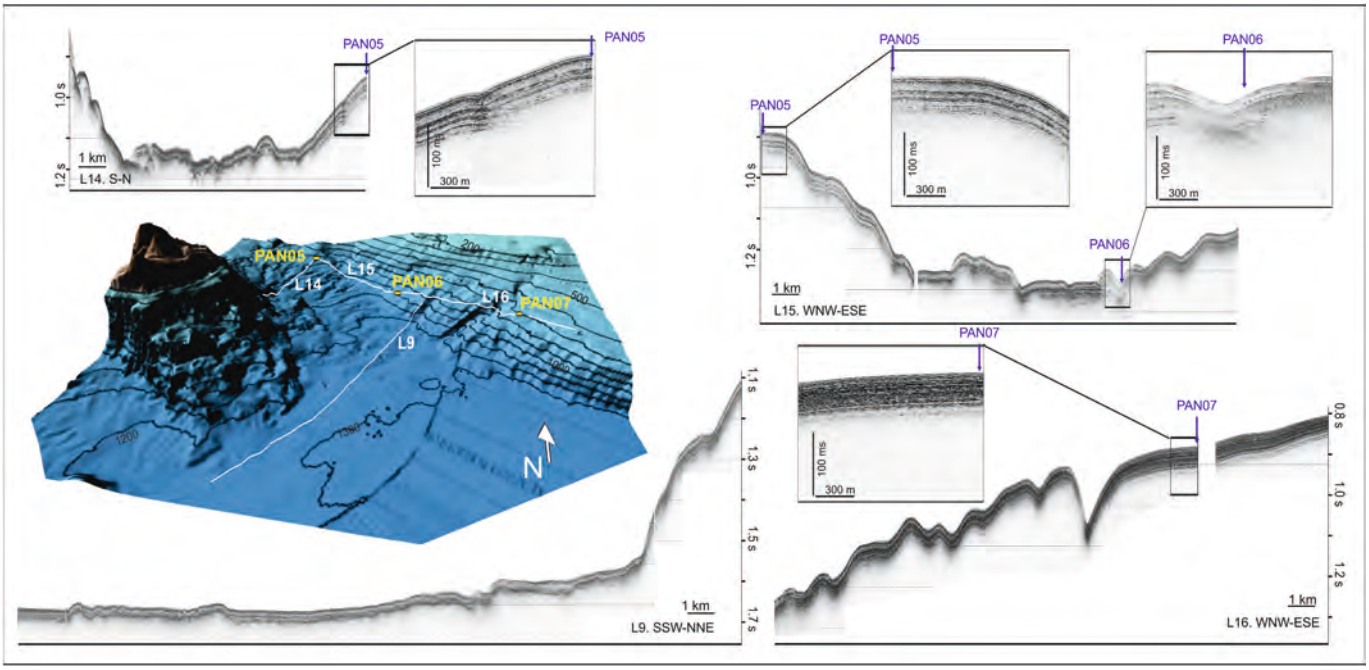

Fig. 3. Chirp profiles recorded to the north-east of Pantelleria island (see Fig. 1b) and location of cores PAN05, PAN06, PAN07.

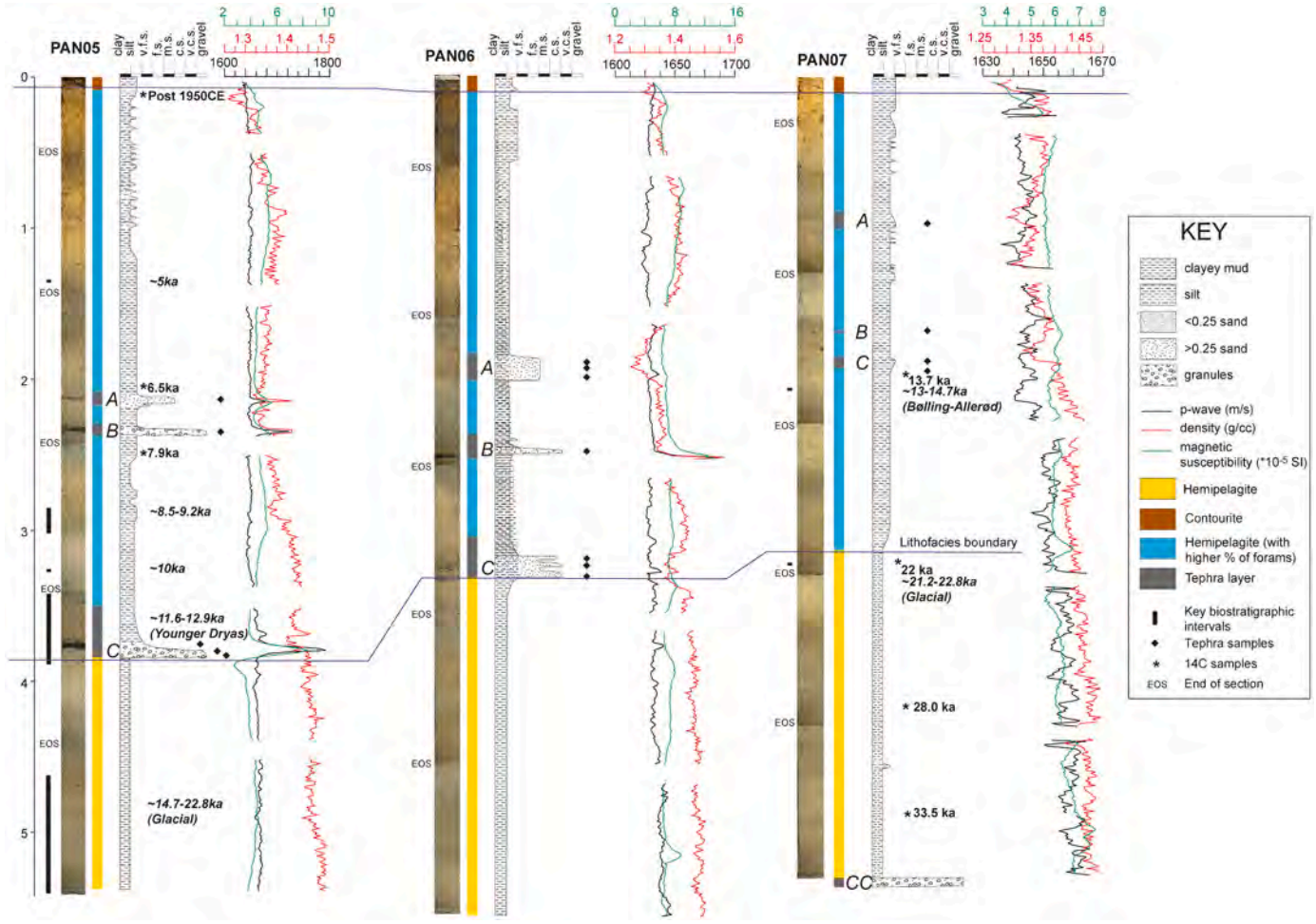

Fig. 4. Logs of cores, with indication of lithology, facies, and analysed tephra layers (see text for details). On the right side, gamma ray density, magnetic susceptibility and P-wave velocity measurements for each core are reported.

deposition (cf. Stow and Piper, 1984).

(4) The tephra layers consist of a mixture of volcanic pumice, glass fragments and black volcanic sand; the relative abundances of the different components vary among the different samples (see Section 4.2). The deposits also show a large granulometric range, from well sorted fine ash to poorly sorted coarser fractions, with sparse volcanogenic granules or pebble-size lapilli set in a very fine ash matrix. Tephra layers have a very distinctive signature regarding physical properties (Freundt et al., 2021). Magnetic susceptibility tends to increase with respect to previous lithofacies, as does p-wave velocity. Gamma ray measurements show repeated sharp positive and negative peaks (Fig. 4). Since there are no lithological changes within these layers, this pattern is interpreted to represent changes in the density related to different degrees of sorting or different content of magnetic minerals from base to top in the thicker tephra layers (see for instance 05C, 06A,06C and 07C in Fig. 4). These changes in physical properties are more pronounced in cores PAN05 and PAN06, where the tephra layers have sharper, possibly erosional, contacts with the hemipelagite above and below. In core PAN07, the tephra appears more dispersed within the sediment and physical properties do not show such distinctive peaks and troughs.

4.1.3. Bio- and chrono-stratigraphy

The bio-stratigraphic framework obtained for selected samples from cores PAN05 and PAN07 (Table 2), considered to have collected a relatively undisturbed, recent sedimentary succession, are based on micropaleontological analyses where the foraminiferal content and preservation allowed this. The bio-stratigraphy is based on planktonic foraminiferal ecozones established in the region and associated approximate calendar ages (Tables 2 and A1 in the Appendix).

Moving from the bottom to top of cores (Fig. 4), the lower section of PAN05 (between 544 and 464 cm) is dominated by species primarily associated with cold sea surface temperatures (SSTs), specifically *Globigerina bulloides*, *Turborotalia quinqueloba* and *Neogloboquadrina incompta*. Coupled with an absence of warmer water species such as *Globigerinoides ruber*, this faunal assemblage is interpreted to be representative of the last glacial period. Very low frequencies (<4%) of *Globorotalia inflata* indicate ecozone 8F (see Table 2 and A1). Similar cold-water assemblages are noted between 384 and 344 cm. However, increasing frequencies of *T. quinqueloba* and a concomitant decrease in *G. ruber* provides evidence of the Younger Dryas climatic event, corresponding to ecozone 6F. Peak frequencies (~40%) of *G. inflata* are observed at 324 cm correlating to a similar peak recorded in core ODP 963D (Sprovieri et al., 2003). Coinciding with small frequencies (<2%) of *Globororotalia truncatulinoides* (sinistral) and an abrupt decline in cold water species (*T. quinqueloba* and *N. incompta*), the faunal assemblage represents the climate amelioration associated with the beginning of the Holocene epoch (ecozone 5F). The faunal assemblage at 304–284 cm is dominated by warm water species. Peak frequencies (~52%) of *G. ruber* are recorded in association with members of the SPRUDTS-group (*Orbulina universa* and *Globoturborotalia rubescens*; Rohling et al., 1993) and *G. inflata*. This assemblage correlates with ecozone 4F, possibly coinciding with the deposition of the Sapropel subunit S1a. Finally, the reappearance of *G. truncatulinoides* occurs at approximately 134 cm in PAN 05. This event is known to occur at approximately 5000

yrs. BP (Margaritelli et al., 2022) and is therefore synonymous with the uppermost part of ecozone 3F.

The lower sample of PAN07 (320–321 cm) is dominated by *N. incompta*, *G. bulloides* and *G.ruber*, with smaller frequencies of *G. glutinata*, *G. scitula* and *T. quinqueloba*. There is a notable absence of *G. inflata*. Clearly representative of glacial conditions, the faunal signal displays similar characteristics to ecozone 8Fa (~21,200–22,800 cal. yrs BP) (Sprovieri et al., 2003). In contrast, the younger of the two samples (208–209 cm) displays a significant reduction in cold water species and an increase in the frequencies of *G. ruber* and *G. inflata.* In association with *G. bulloides,* the faunal assemblage possibly correlates to ecozone 7F representative of the Late Glacial Bolling-Allerod period (~13,000–14,700 cal. yrs BP) (Sprovieri et al., 2003).

The bio-stratigraphy is in tune with the age range provided by seven calibrated ages obtained by radiocarbon dating of selected samples from cores PAN05 and PAN07 (Table 3 and Fig. 4) and, although data are not so dense to allow to draw a continuous age model, the overall chrono-stratigraphic framework for the cores is consistent with the identified ecozones. Overall, the upper foraminifera-rich hemipelagite is bracketed by the top radiocarbon age in PAN05 indicating modern sediment (Post 1950 CE), and the top of the lower hemipelagite in core PAN07 dated at 22,010 cal yr BP at 320–321 cm. Radiocarbon dates within the upper hemipelagites include 6,507 cal yr BP at 205-206 and 7870 cal yr BP at 255–256 cm in PAN05, and 13,730 cal yr BP at 195–196 cm in PAN07 (Table 3). These dates are supported by the identified ecozones and the bio-stratigraphical samples that suggest that the upper hemipelagite was deposited since the Late Pleistocene (as for core PAN07) and throughout the Holocene (Table 3). The clear lithofacies correlation of both cores with PAN06 (Section 4.1.2) allows for an approximate extrapolation of the stratigraphic framework to the lithofacies in this core too.

It appears that the transition between the glacial and interglacial period (from bottom to top in the cores) was characterized by the passage from the deposition of finer-grained hemipelagites (labelled in yellow in Fig. 4), as observed below tephra layer 05C in PAN05, below tephra layer 06C in PAN06 and above the bio- and chrono-stratigraphical sample at 320–321 cm in PAN07, to foraminifera-rich, coarser grained hemipelagites in the upper part of the cores (labelled in blue in Fig. 4). There is a difference between cores PAN05 and PAN06 compared to PAN07 in the transition between lower and upper hemipelagites. In core PAN07 the foraminifera-rich, coarser grained hemipelagite is also present below the tephra layer C, while in PAN05 and PAN06 below their respective tephra layers C, there is a sudden transition to the lower, finer-grained hemipelagite. The very sharp, possibly erosional, lower contact for these tephra layers suggest that there may be a sedimentary hiatus just below these tephras that could account for the different lithostratigraphy in these cores below tephras C compared to core PAN07 (i.e. sudden transition into the lower hemipelagites).

From radiocarbon calibrated ages, an average sedimentation rate of ~0.32 mm/y in PAN05 and ~ 0.15 mm/yr in PAN07 is estimated for the upper hemipelagite. The calibrated ages in the lower hemipelagite in PAN07 (22,010 cal yr BP at 320–321 cm, 28,020 cal yr BP at 420–422 cm and 33,520 cal yr BP at 484–487 cm, Table 3) and the identified ecozones (Table 2) suggest that this facies was deposited during the last glacial period at an average sedimentation rate of ~0.14 mm/yr in PAN07 (the only core where there are enough chronostratigraphic data for this calculation).

4.2. Sedimentological characteristics and composition of tephra layers

Nine tephra-rich layers were identified and sampled in the cores (Table 4).

The thickest tephra layers (05C, 06A and 06C, thickness $\geq$ 10 cm; Table 4) were sampled at the top and base and in intermediate positions, whereas the thinner tephra layers were only sampled once. In core PAN07 a further sample (07-CC) was taken from the coarse-grained volcanic deposit recovered in the core catcher. It contained a large amount of cm-scale pumice and scoria fragments (Fig. A1 in the Appendix) that was probably responsible for the relatively limited corer penetration at this site.

In most cases tephra are cm- to dm-thick layers, often showing normal grading and sharp base and/or top contacts; at times the contacts are gradual (Fig. 4 and Table 4). Grain size is variable from ash to lapilli (Table 4).

Volcanic material has been assumed as derived from primary tephra layers for its homogeneity, both compositional and lithological: tephra layers are composed at 90–100% of fresh juvenile material mostly represented by medium to fine-grained pumices and glass shards, with variable morphology and vesicle content (Fig. 5). The different types of pumice grains range from highly vesicular to fibrous-elongated grains with spheroidal and tubular vesicles, respectively (Fig. 5A and C). Colours range from light to dark grey. Non-vesicular, blocky fragments, such as dark scoriae and obsidian fragments (Fig. 5B), glass with sub-rounded vesicles (Fig. 5D) or crystals are also present in lower percentages. In sample PAN07-CC, recovered in the core catcher, vesicular pumiceous lapilli have been observed and singularly picked for the analyses (Fig. A1 in the Appendix). They consist of cm- to mm- grains with irregular morphology, from equigranular to fibrous-elongated.

The major and minor elements composition of the tephra layers recognized in cores PAN05, PAN06, PAN07 and in the core catcher of core PAN07 is reported in Tables 5 and 6, respectively.

The results from the EMPA-WDS and EDX analysis of the tephra layers (see also file in the Supplementary material with the original data set) show that, despite the different morphologies and sizes, the glassy fragments from the three cores display a homogeneous chemical composition defining a unique population of rhyolites, with SiO_2 concentration between ~72 and ~74 wt% (Fig. 6). All these tephra have a peralkaline composition (peralkalinity index, PI in the range 1.7–2, Table 5) which makes them classifiable as pantellerite in the FeO_t vs Al_2O_3 diagram (Fig. 7).

Sample PAN07-CC from the Core-Catcher of PAN_07 has revealed different composition from the other tephra layers: it is bimodal and characterized by rhyolitic (mainly) and trachytic populations (Fig. 8a). The peralkaline character of all compositions (PI = 0.9–1.1 for trachytes and 1.6–1.9 for rhyolites, Table 6) makes them classifiable as pantellerite and comenditic trachyte, respectively (Fig. 8b). This deposit also contains a small fraction of microcrystals, locally included in pumice grains. This mineral assemblage includes alkali feldspar (Na-rich sanidine and anorthoclase), clinopyroxene (aegirine-augite), aenigmatite and Ti-rich magnetite as accessories, similar to that of peralkaline rocks on the island (Wolff and Wright, 1981; Civetta et al., 1988; Avanzinelli et al., 2004; Lanzo et al., 2013).

4.3. Tephra stratigraphic position and possible correlation

As indicated in Section 4.1, the chronostratigraphic framework for the studied cores, reconstructed from micropaleontological analyses and radiocarbon dates (Tables 2 and 3), allows the identification of three time intervals that include the recognized tephra layers:

a) Interval 1 – Mid-Holocene between about 6500 and 7900 cal yr BP, including tephra 05A, 05B, 07A (Fig. 4). Despite the lack of absolute age determinations for core PAN06, we tentatively propose that tephra 06A and possibly 06B could be also included in this interval, based on their location within the upper hemipelagite and the relative reconstructed stratigraphic correlation among the 3 cores.
b) Interval 2 – Early Holocene/end of Late Glacial, around the Younger Dryas and the Bølling-Allerød period (between 11,600 and 13,700 cal yr BP): tephra 05C (likely deposited around the Younger Dryas or just before) and, possibly, also 06C, both located just at the transition between the two different types of hemipelagite (Fig. 4), interpreted as corresponding to the transition between glacial and interglacial; tephra 07C (calibrated age below this tephra is 13,730 cal yr BP) and

Table 4
List of tephra layers recognized and sampled in the cores and main sedimentological and lithological characteristics.

Core	Tephra layer	Thickness (cm)	Sample depth (cm)	Lithology	Characteristics of juvenile material
PAN05	05A	210–218 (8)	214–215	Coarse to medium ash; net contact at base and top	Abundant pumice fragments (sub-mm to mm-size) with irregular morphology, either vesicular or fibrous-elongated. Rare glass shards and crystals.
	05B	232–236 (4)	235–236	Coarse ash and lapilli; net/irregular contact at base and top	Pumice fragments of different size (up to 1 cm), irregular morphology, mostly vesicular and rare fibrous-elongated ones. Rare glass shards and crystals.
	05C	371–381 (10)	372–373 375–376 379–381	Coarse to fine ash (fining upward); net contact at base and top	Pumice fragments of different size (sub-mm to mm-size at the base), irregular morphology, vesicular or fibrous-elongated. Rare glass shards, crystals and lithics.
PAN06	06A	186–200 (14)	191–192 194–195 197–198	Coarse to fine ash (fining upward); net contact at base	Pumice fragments of different size (sub-mm to mm-size at the base), mostly vesicular and (rare) fibrous-elongated. Rare glass shards and crystals.
	06B	251–259 (8)	252–253	Medium to fine ash (lateral passage); net contact at base and top	Pumice fragments of different size (mm- to sub-cm size), irregular morphology, vesicular and (rare) fibrous-elongated. Rare glass shards and crystals.
	06C	320–339 (19)	321–323 327–329 332–334	Fine ash at base and top, lapilli and crystals in a silty matrix in the middle; erosive contact at base	Pumice fragments of different size (mm- to sub-cm size at the base), irregular morphology, vesicular or fibrous-elongated, less fresh appearance with muddy matrix within the interstices. Rare glass shards, crystals and lithics (apart from sample 327–329: mostly crystals, scarce fibrous-elongated pumices and glass shards).
PAN07	07A	86–95 (9)	90–91	Fine to medium ash + sparse larger clasts (coarsening upward); net contact at base	Pumice fragments (sub-mm to mm-size), vesicular or tubular. Rare glass shards and crystals.
	07B	169–170 (1)	169	Medium to fine ash	Highly vesiculated pumices fragments (sub-mm and sub-cm size, irregular shape) with crystal inclusions. Rare crystals.
	07C	179–187 (8)	180–181 185–186	Sparse lapilli in fine ash	Two pumice fragments (sub-cm size), angular and sub-rounded shapes. Low amount of fibrous-elongated pumice fragments (mm- to sub-cm size)
	07-CC	–	CC	Lapilli and ash	Pumice fragments of cm- to mm-size and irregular morphology, equigranular texture, either vesicular or fibrous-elongated.

possibly 07B that, according to estimated sedimentation rate, has an age of around 11,900 cal yr BP).

c) Interval 3 – older than 37,000–38,000 cal yr BP: no tephra layers were observed in the lower part of the three studied cores within the lower, foraminifera-poor, hemipelagite deposited during the last glacial period, apart from the volcanic material sampled in the core catcher (Fig. 4). Radiocarbon ages obtained for the lower part of core PAN07 give an age of 33,520 cal yr BP at 484–487 cm (Table 3). On the basis of the estimated sedimentation rates for the lower hemipelagite in core PAN07, the tephra sampled in the core catcher of PAN07 (07-CC) can be considered older than 37,000–38,000 cal BP.

Possible correlations between tephra layers recognized in interval 1 (05A, 06A and 07A; 05B and 06B) can be proposed with good confidence. As for tephra in interval 2, 05C and 06C could be confidently correlated between them due to their comparable stratigraphic position, close to the lithological transition between the upper and lower hemipelagites (Fig. 4). For tephra 07C, the correlation is also supported by bio- and chronostratigraphic information (Table 2 and Fig. 4), despite its different position with respect to litho-stratigraphy. This is discussed in Section 5.2. In the next section, in fact, we discuss possible correlations among the analysed tephra layers and the known eruptive history of Pantelleria, also in the light of the effects of the marine setting on the stratigraphy of the sampled sedimentary succession and on tephra preservation.

5. Discussion

The lithological characteristics of the tephra sampled in the three cores, with very high concentration of juvenile material (especially pumice and glass shards) and scarce to absent biogenic component, together with the homogeneous geochemical signature, support their primary nature (see also Freundt et al., 2021). This is also supported by the low variability in the sedimentary characteristics of the sampled layers, some of which are fining upward (likely due to settling through the water column; Hopkins et al., 2020) and show sharp bottom surfaces in sediment cores (Cassidy et al., 2014). Moreover, the peculiar coarse-grained texture of the volcanic deposit recovered in the core catcher of core PAN07, mostly made of cm- scale pumiceous fragments (Fig. A1 in the Appendix), suggests an origin related to an eruption of considerable intensity from a proximal source. In the following subsections, we propose the possible correlations of the observed tephra layers with the known eruptive history of Pantelleria, despite possible limitations in establishing proximal and distal correlations using major element may arise in comparing different dataset. Most literature data on proximal deposits of the Italian magmatic provinces, in fact, still rely on whole rock geochemistry, which represents the average of both melt and phenocrysts/lithic fragments obtained through different analytical techniques (ICP-MS, INAA, X-ray fluorescence) (Tamburrino et al., 2012). We also propose a correlation between the deposit recovered in the core catcher of PAN07, and the marine distal tephra Y-6 widely reported in literature.

5.1. Correlation of tephra layers with the volcanic activity of Pantelleria and implications on the reconstruction of eruptive history

5.1.1. Correlation with eruptive activity in the last 13.7 ka

Tephra layers deposited at the end of the last Glacial period and in the Holocene (Intervals 1 and 2 in Section 4.3) all show a very homogeneous geochemical signature corresponding to rhyolitic composition (pantellerites) with PI in the range 1.7–2 (Fig. 6 and Table 5), typical of the peralkaline silicic volcanic rocks of Pantelleria (see Section 2). These tephra can be associated with the most recent silicic eruptive cycles recognized on Pantelleria Island in the post-GT history, when pantelleritic magma once again dominated volcanic activity (Lanzo et al., 2013). In particular, time intervals 1 and 2 correspond well with the last

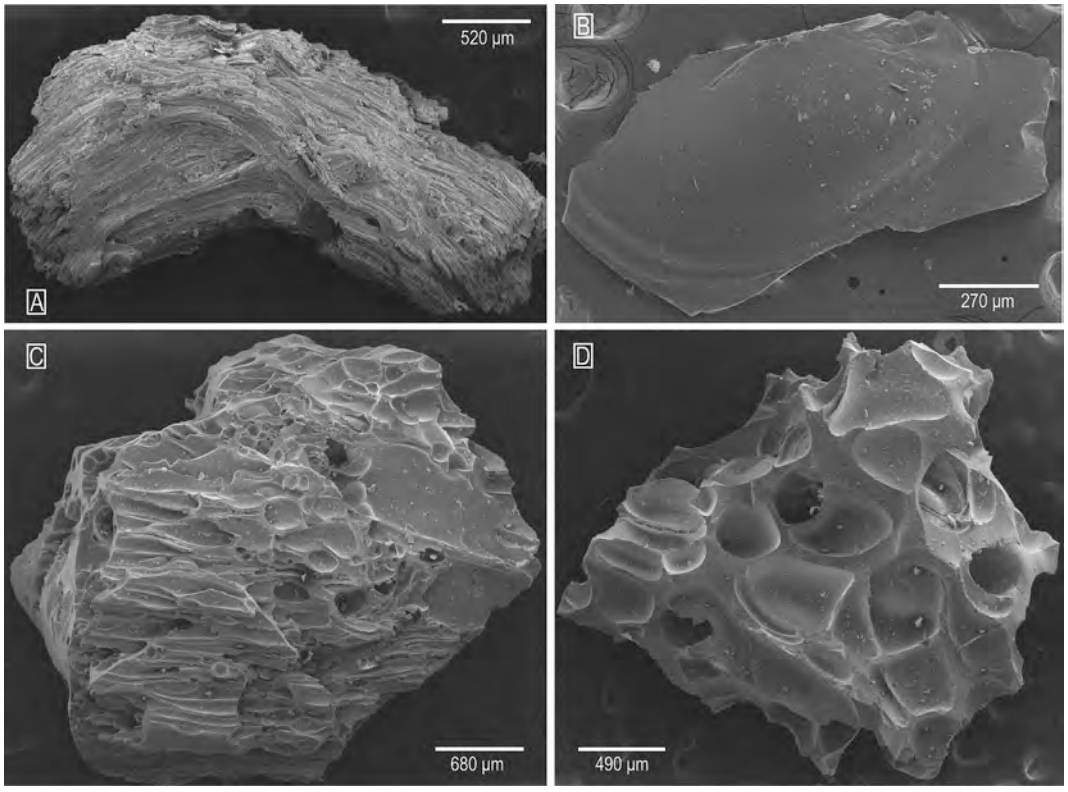

Fig. 5. Selected SEM images of glass shards and pumice fragments picked from the analysed samples: (A) and (C) highly vesicular, fibrous elongated pumice fragments (from tephra 05C); (B) platy glass shard (from tephra 06B); (D) glass fragment with sub-spherical blisters (from tephra 05C).

(VI) and the penultimate (V) peralkaline eruptive cycles (Civetta et al., 1988; Civetta, 1998; Avanzinelli et al., 2004; White et al., 2009; Gioncada and Landi, 2010; Di Genova et al., 2013) which have been radiometrically dated at 5–10 ka and 12–14 ka, respectively (Mahood and Hildreth, 1986; Civetta et al., 1988). While the tephra found in the studied sediment cores display comparable (slightly more acid) pantelleritic compositions with respect to deposits inland (whole rock analyses, Figs. 9 and 10), trachytic ones are not represented. This might be partly explained by the fact that trachytic products are relatively less diffused also in the related units outcropping on the island, where comenditic trachyte occurs primarily as magmatic enclaves in pantellerite lavas (White et al., 2009).

More recently, based on paleomagnetic dating on samples from products of the VI cycle, Speranza et al. (2010) constrained the duration of the most recent eruptive cycle in a short time span of a few centuries around 6.0 ka, and questioned the occurrence of several small peralkaline eruptions of different age punctuating the 5 to 10 ka eruptive activity at Pantelleria, as proposed by previous reconstructions. These authors also propose that a possible interval of volcanic quiescence, 4–8 ka long, occurred between eruptive cycles V and VI. A chronologic refinement for the post-caldera silicic activity of Pantelleria comes from the high-resolution $^{40}Ar/^{39}Ar$ chronostratigraphy of Scaillet et al. (2011), for which the four cycles subdivision appears questionable. These authors point out that the products of the most recent cycle(s) overlie a dark-red paleosoil (DRP) marking the (only recognizable) volcanic stasis at ~12–14 ka ago. This latter probably represents an upper age limit for the tephra we recognize in the upper hemipelagite (corresponding to time intervals 1 and 2, <13.7 ka). Conversely, regarding the possible overall decline in eruptive frequency and rate (but without major changes in the eruptive style) between the pre- and post- DRP activity claimed by Scaillet et al. (2011), we cannot confirm this decreasing trend since in the studied cores we do not find evidence of tephra older than 13.7 cal kyr BP, except for the deposit sampled in the core catcher of PAN07 (tephra 07-CC, see Section 5.1.2). However, this might be due to lack of preservation of primary deposits, as it is discussed in Section 5.2. Moreover, we concentrated our analyses on distinctive tephra layers visible to the naked eye, and not to possible cryptotephra eventually present in the cores. Indeed, some slight peaks in magnetic susceptivity are visible at the base of core PAN06 and PAN07, but cannot be associated with evident changes in other physical parameters such as density or p-wave values (Fig. 4). A more precise stratigraphy and dating of the sampled marine sedimentary succession, thus, might provide an improved tephra synchronization with the terrestrial counterparts.

5.1.2. Correlation with the Green Tuff (GT)

The chronological constraints for the base of core PAN07 indicate that tephra 07-CC may be dated as older than 37,000–38,000 cal yr (Section 4.3), but we cannot exclude the occurrence of a hiatus at the base of the core due to erosion/reworking of the sedimentary succession. The non-conservative sampling trough gravity coring, that was probably not effective in penetrating this coarse-grained unit (sample 07-CC comes from the core catcher and is out of the core) may be responsible for the incomplete recovery of the marine succession at its base.

Nevertheless, the peculiar bimodal composition shown by tephra 07-CC, mostly rhyolitic (pantellerite) and trachytic, (Fig. 8a and Table 6) supports a correlation with that of the marine distal tephra Y-6 and that of the GT proximal area on the island (whole rock) (Figs. 11 and 12). This composition is, in fact, distinctive among the younger tephra layers in the Mediterranean as reported by many studies (Table A2 in the Appendix) that associate it to Pantelleria and, in particular, to the GT large-magnitude eruption. A similar bimodal composition is found, in fact, in the GT deposits on the island (Civetta et al., 1988; Civetta, 1998; Avanzinelli et al., 2004; White et al., 2009; Lanzo et al., 2013; Di Genova et al., 2013; Scaillet et al., 2013) and in the well-known distal marine and lacustrine equivalent of the GT (tephra Y-6; Keller et al., 1978;

Table 5
Major and minor elements composition of analysed glasses (wt%) from tephra samples along the studied cores. Number in parentheses after "mean(x)": number of analysed points; PI: peralkalinity index; bdl: below detection limits.

PAN-05	SiO2	TiO2	Al2O3	FeO	MnO	MgO	CaO	Na2O	K2O	P2O5	Tot*	ALK	PI
PAN-05A (EMPA)													
mean(15)	72.24	0.35	7.82	8.49	0.32	0.04	0.42	5.93	4.36	0.01	98.88	10.29	1.85
st-dev	0.34	0.03	0.22	0.18	0.04	0.02	0.04	0.17	0.10	0.01	1.80	0.16	0.10
PAN-05B (EMPA)													
mean(29)	72.53	0.35	7.56	8.47	0.32	0.04	0.38	5.93	4.40	0.02	98.03	10.33	1.92
st-dev	0.44	0.04	0.12	0.23	0.05	0.02	0.04	0.33	0.12	0.02	1.30	0.72	0.20
PAN-05C (EMPA)													
mean(23)	72.63	0.35	7.47	8.44	0.30	0.05	0.40	5.92	4.41	0.02	97.57	10.33	1.94
st-dev	0.25	0.02	0.09	0.16	0.04	0.01	0.04	0.15	0.07	0.02	1.23	0.19	0.10
PAN-05C (EDX)													
mean(17)	72.86	0.13	8.28	8.06	0.17	0.09	0.19	5.68	4.54	bdl	95.67	10.85	1.72
st-dev(2 s)	0.41	0.08	0.09	0.11	0.06	0.07	0.03	0.22	0.04	bdl	1.67	0.24	0.08
PAN-06	SiO2	TiO2	Al2O3	FeO	MnO	MgO	CaO	Na2O	K2O	P2O5	Tot*	ALK	PI
PAN-06A (EMPA)													
mean(21)	72.40	0.35	7.65	8.37	0.32	0.05	0.42	6.04	4.38	0.02	98.49	10.42	1.92
st-dev	0.30	0.05	0.24	0.16	0.05	0.01	0.04	0.10	0.07	0.02	1.34	0.09	0.14
PAN-06A (EDX)													
mean(36)	72.31	0.15	8.37	8.10	0.20	0.13	0.22	6.02	4.5	bdl	96.50	10.51	1.76
st-dev	0.30	0.06	0.13	0.14	0.06	0.07	0.04	0.24	0.07	bdl	1.84	0.24	0.1
PAN-06B (EMPA)													
mean(18)	72.63	0.34	7.44	8.43	0.30	0.05	0.41	5.95	4.42	0.02	97.81	10.37	1.96
st-dev	0.52	0.06	0.24	0.26	0.06	0.04	0.12	0.30	0.14	0.04	2.03	0.34	0.12
PAN-06C (EMPA)													
mean(18)	72.61	0.36	7.54	8.37	0.29	0.05	0.39	5.95	4.43	0.03	97.32	10.38	1.94
st-dev	0.52	0.06	0.38	0.24	0.08	0.04	0.06	0.22	0.20	0.04	1.39	0.34	0.12
PAN-06C (EDX)													
mean(50)	72.76	0.14	8.26	7.95	0.18	0.12	0.23	5.86	4.49	bdl	96.75	10.35	1.76
st-dev	0.28	0.06	0.12	0.17	0.06	0.08	0.04	0.20	0.06	bdl	1.30	0.19	0.10

Table 6
Major and minor elements composition of analysed glasses (wt%) from sample PAN07-CC. Number in parentheses after mean(x): number of analysed points; PI: peralkalinity index; bdl: below detection limits.

PAN-07	SiO2	TiO2	Al2O3	FeO	MnO	MgO	CaO	Na2O	K2O	P2O5	Tot*	ALK	PI
PAN-07A (EMPA)													
mean(13)	72.71	0.33	7.57	8.38	0.31	0.04	0.42	5.84	4.37	0.02	98.01	10.21	1.89
st-dev	0.52	0.06	0.14	0.32	0.08	0.02	0.10	0.58	0.16	0.04	2.02	0.54	0.14
PAN-07B (EMPA)													
mean(20)	72.73	0.34	7.36	8.41	0.28	0.05	0.40	5.99	4.40	0.03	97.40	10.40	1.99
st-dev(2 s)	0.34	0.06	0.36	0.30	0.08	0.04	0.06	0.30	0.16	0.06	1.60	0.36	0.16
PAN-07C (EMPA)													
mean(6)	72.65	0.37	7.61	8.31	0.28	0.05	0.41	5.92	4.40	0.02	96.51	10.31	1.92
st-dev	0.76	0.02	0.92	0.32	0.06	0.02	0.12	0.60	0.26	0.04	2.05	0.78	0.34
PAN-07C (EDX)													
mean(9)	72.60	0.11	8.32	8.09	0.16	0.13	0.25	5.91	4.44	bdl	95.02	10.35	1.75
st-dev	0.36	0.06	0.20	0.10	0.08	0.06	0.06	0.42	0.06	bdl	1.76	0.39	0.22

Cornette et al., 1983; Narcisi and Vezzoli, 1999; Margari et al., 2007; Paterne et al., 2008; Tamburrino, 2008; Vogel et al., 2010; Damaschke et al., 2013; Tamburrino et al., 2012, 2016; D'Antonio et al., 2016; Zanchetta et al., 2018) (Table A2 and Fig. 11). On land, the GT compound unit is divided into members and has a continuous trend from pantellerites (basal units) to comenditic trachytes and trachytes at the top (Orsi and Sheridan, 1984; Mahood and Hildreth, 1986; Civetta et al., 1988; White et al., 2009), with a parallel decrease in PI from 1.71.8 to 1.0 from base to top (White et al., 2009; Scaillet et al., 2013). The vertical sampling of the GT sequence on the island shows, in fact, that mineral and glass composition vary rather gradually throughout the sequence (Williams, 2010). Pantellerite was largely the dominant

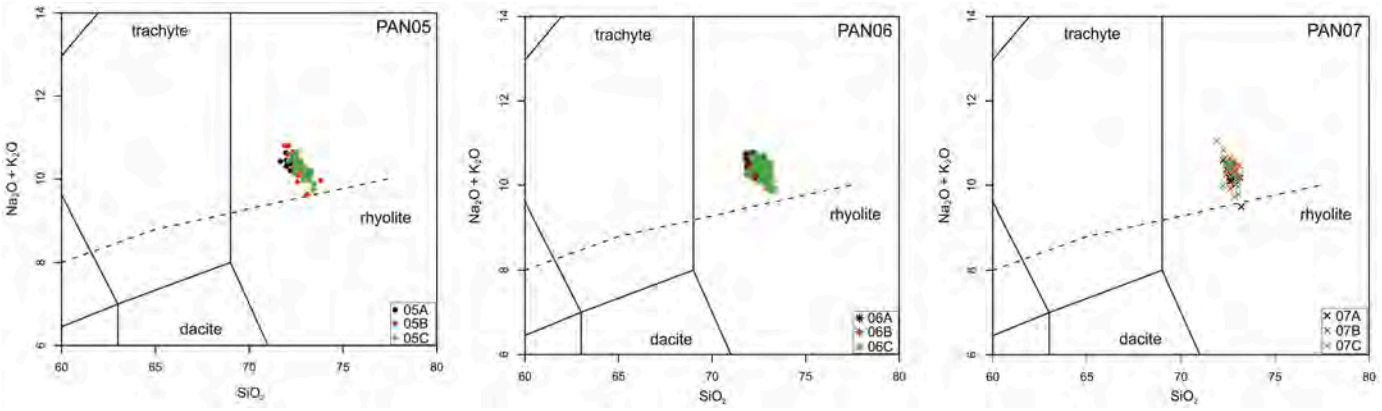

Fig. 6. Total alkali/silica (TAS) classification diagram (Le Bas et al., 1986) showing the chemical composition of the analysed tephra from core PAN05, PAN06 AND PAN07.

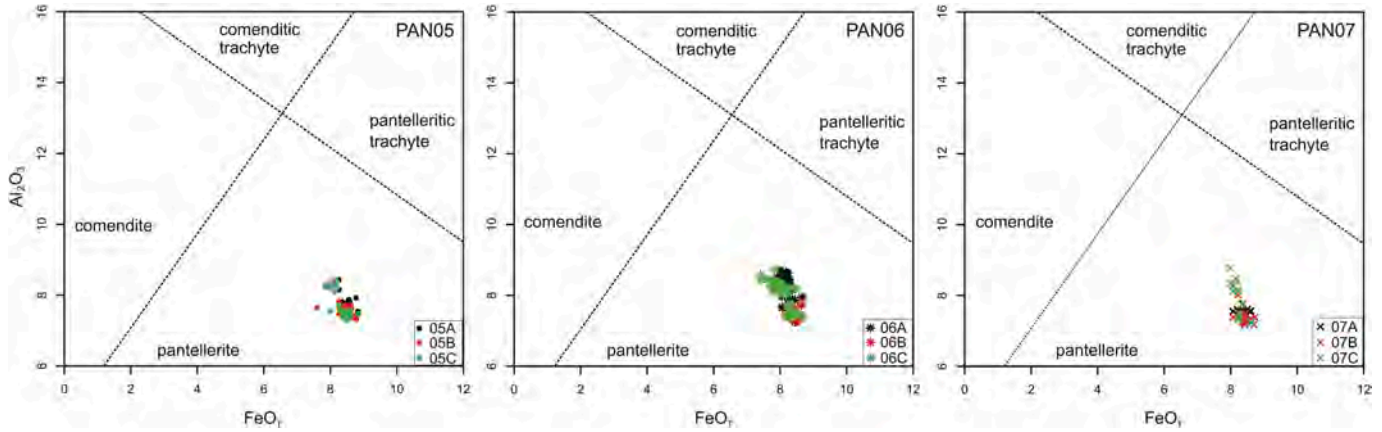

Fig. 7. FeO_t/Al_2O_3 classification diagram for peralkaline products (MacDonald, 1974) for tephra analysed in cores PAN05, PAN06, PAN07. Symbols as in Fig. 6.

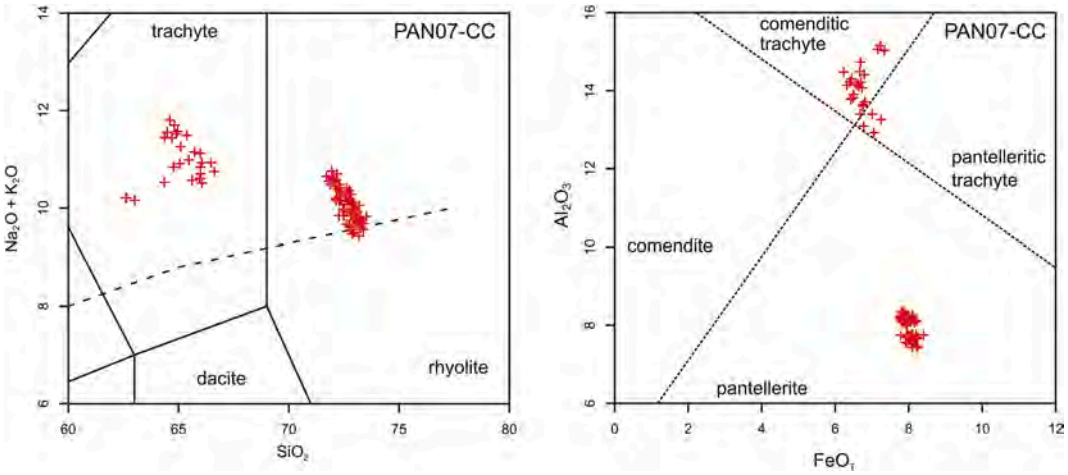

Fig. 8. (a) Total alkali/silica (TAS) classification diagram (Le Bas et al., 1986) and (b) FeO_t/Al_2O_3 (Macdonald, 1974) for tephra PAN07-CC.

magma, while the less evolved trachyte magma originated a small-volume pyroclastic unit emplaced at the top of the GT sequence (Lanzo et al., 2013; Cinquegrani et al., 2022). This compositional zoning of the GT is important to consider for accurate identification of distal equivalents which may represent a mixture between the pantellerite/-trachyte end members during dispersal and deposition (Scaillet et al., 2013).

A continuous trend from pantellerites to comenditic trachytes and trachytes of the latter group is not fully represented in tephra 07-CC. In particular, our data match very well the rhyolitic group of compositions reported in the literature, and also extend in the field of the trachytic group (Figs. 11 and 12). The latter appears generally less documented in distal tephra, where only the more differentiated terms were recovered in some locations (see Fig. 11 and Table A2 in the Appendix). Trachytic compositions are, instead, well documented in a GT-related marine tephra sampled at ODP Site 963A coring site (Fig. 1a, 11 and 12), i.e., in

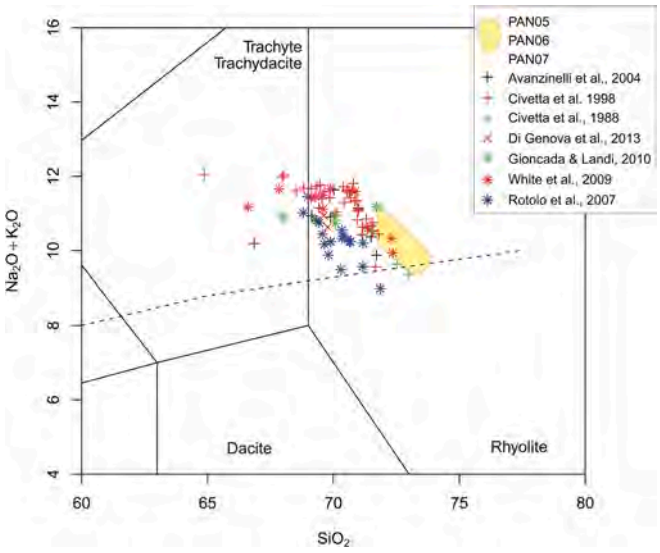

Fig. 9. Total alkali/silica (TAS) classification diagram (Le Bas et al., 1986) comparing tephra from cores PAN05, PAN06, PAN07 with literature data for the post-GT units (see text for details).

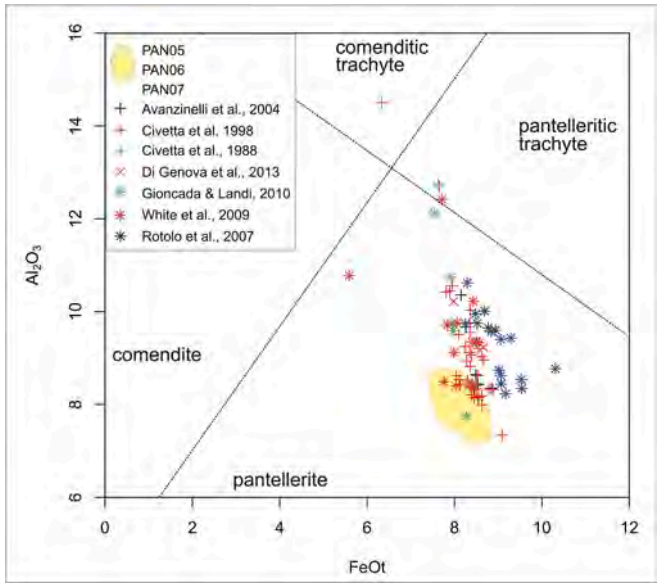

Fig. 10. FeO_t/Al_2O_3 classification diagram comparing tephra from cores PAN05, PAN06, PAN07 with literature data for the post-GT units.

a relatively proximal location about 100 km east of Pantelleria: here the prevalence of rhyolitic composition at the bottom and of trachytic ones at the top of the tephra was noted, the latter having a lower degree of differentiation than in more distal deposits (Tamburrino, 2008; Tamburrino et al., 2012). Since the original structure of our sample 07-CC, recovered in the core catcher, was not preserved, and only the superficial part of the deposit was picked by the gravity corer, we cannot discuss any vertical compositional zoning in this tephra. Nevertheless, the finding of a mixture between the pantellerite/trachyte end members in tephra 07-CC is worth mentioning, since it appears to increase the compositional range compared to that recorded in more distal marine tephra (Figs. 11 and 12). Also, the association of peralkaline glass shards with aenigmatite and other minerals in our samples (Na-rich sanidine, anorthoclase, aegirine-augite) is consistent with the mineralogy and composition of the GT (Wolff and Wright, 1981; Avanzinelli et al., 2004; Anastasakis and Pe-Piper, 2006; Lanzo et al., 2013; Scaillet et al., 2013).

The petrochemical and mineralogical characteristics of tephra 07-CC thus support its correlation with the GT eruption, here sampled in a near-vent location (about 15–30 km from the source area). Pumice falls associated with ignimbrite-forming eruptions are rare and not widespread, and the GT event is considered one of them (Rotolo et al., 2021). The coarse-grained texture of the deposit we have sampled at the base of core PAN07, entirely made of coarse ash to lapilli-size volcanic juvenile fragments (see Fig. A1 in the Appendix), suggests a short transportation and rapid deposition, as is the case of other co-ignimbrite fallout deposits in proximal-median areas (Wuthke et al., 2016; Hopkins et al., 2020; Di Roberto et al., 2020). The grain size and juvenile components of a tephra fall deposit, in fact, are dependent on the distance from source eruption and wind effects during transportation (Hopkins et al., 2020). The characterization of this tephra may thus provide new evidence on the GT explosive event and near-vent facies and dispersion pattern of related erupted volcanic material, up to now documented mostly in its distal (more fine-grained) facies by lacustrine and marine tephra collected in various parts of the Mediterranean (Keller et al., 1978; Narcisi and Vezzoli, 1999; Margari et al., 2007; Vogel et al., 2010; Tamburrino et al., 2012, 2016; Zanchetta et al., 2018).

5.2. *Tephra preservation in the marine environment and implications on the record of eruptive activity*

Several intervening factors affect the deposition and preservation of tephra and cryptotephra deposits in the marine realm, posing main critical issues on related volcanological and paleoclimate research (Totaro et al., 2022). Primary fallout through diffuse vertical gravity currents is one of the possible mechanisms of tephra deposition (Carey, 1997; Manville and Wilson, 2004; Cassidy et al., 2014), increasing the particle settling velocity in the water column and possibly reducing the effects of dispersal and sorting by ocean currents (Hopkins et al., 2020). The marine environment in which the tephra are deposited has, in fact, a large influence on the thickness and characteristics of the units, as stratigraphic gaps, bioturbation processes, erosion by marine currents may affect the sedimentary sequence (Hopkins et al., 2020; Totaro et al., 2022).

In this study, sediment cores were retrieved from the NW-SE oriented escarpment that forms the north-eastern margin of the Pantelleria Graben at depth over 650 mwd, so in a relatively higher position with respect to the basin, although not properly on morphological highs.

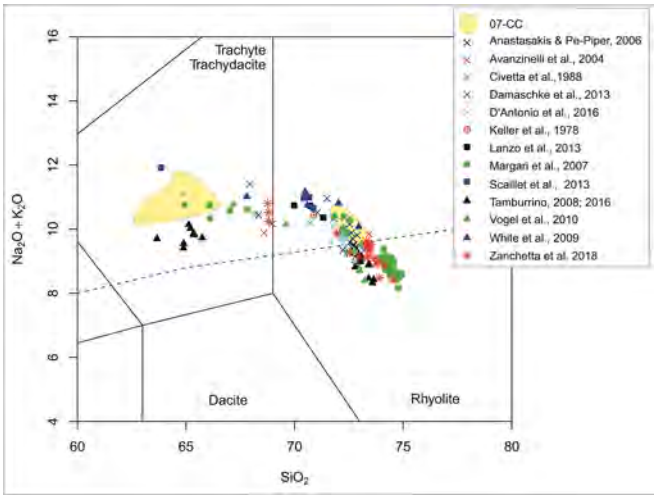

Fig. 11. Total alkali/silica (TAS) classification diagram (Le Bas et al., 1986) comparing deposit sampled in the core catcher of PANO07-CC (yellow fields) with literature data for the GreenTuff distal tephra and whole rock units (see text for details). (For interpretation of the references to colour in this figure legend, the reader is referred to the web version of this article.)

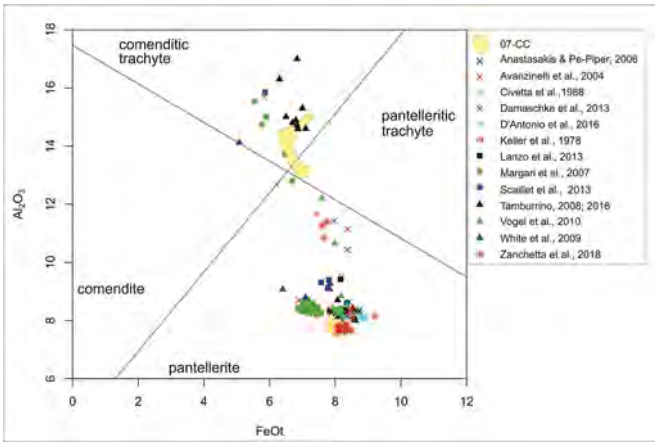

Fig. 12. FeO_t/Al_2O_3 classification diagram comparing deposit sampled in the core catcher of PANO07-CC (yellow fields) with literature data for the Green-Tuff distal tephra and whole rock units (see text for details). (For interpretation of the references to colour in this figure legend, the reader is referred to the web version of this article.)

Seismoacoustic characterization and reconstructed stratigraphy suggest the occurrence of relatively undisturbed recent sedimentation in at least two of the coring sites (PAN05 and PAN07). However, different sedimentation rates are estimated for the two sampled sedimentary successions on the base of the reconstructed chrono- and bio-stratigraphy: 0.32 mm/y and ~0.15 mm/y for PAN05 and PAN07, respectively, for the post-glacial and Holocene; ~0.14 mm/y for PAN07 during the last glacial period. This suggests that differences in setting/depth between the two coring sites may have played a role on the recent sedimentation (and/or on the deposits preservation), besides paleo-environmental changes recorded by the sedimentary succession (glacial and interglacial stages).

For instance, the lower depth of the PAN07 coring sites with respect to PAN05 may partly explain the lower sedimentation rate of the latter one. Coring site PAN07 is located on top of a terraced morphology, at about 668 mwd, a depth that would roughly correspond to the interface between LIW (200–700 mwd) and EMDW (>700 mwd) water masses (see Section 2.2). As witnessed by the occurrence of contouritic drift system on the seabed down to 600 m water depth in the northwesternmost part of the Pantelleria basin (Martorelli et al., 2010), oceanographic effects related to the two water masses should be accounted as potentially affecting the sedimentary record, and might relate to the lower sedimentation rate recorded at the PAN07 site. Effects of the deep and intermediate LIW current activity on enhanced sediment dispersal are also suggested by Kuhlmann et al. (2015) and Gauchery et al. (2021) for sedimentary sequences drilled on the Southern Sicilian margin. In contrast, PAN05 and PAN06 are located in a deeper setting of the slope (750–990 m mwd), being comprised within the area swept by the EMDWL (Fig. 1). The oceanographic control would be less energetic here, allowing higher sedimentation rates and the preservation of finer-grained deposits. These differences in settings among the coring sites can clearly have implications in terms of preservation potential of tephra in the sedimentary successions, as the volcanological record may be incomplete and this is something to consider when studying marine tephra.

6. Conclusions

Near-vent primary volcanic deposits can provide additional information, with respect to distal tephra layers, for reconstructing a comprehensive eruption record of volcanoes (Cassidy et al., 2014; Monaco et al., 2022). Distal tephra deposits commonly provide detailed and undisturbed records of explosive eruptions far away from the volcanic source, representing important markers for dating and correlating sedimentary successions. On the other hand, the comparison with proximal tephra may enlarge the knowledge of eruptive facies and processes and may provide further age constraints, thus supporting the benefit of a multi-location approach to tephrochronology (Pizer et al., 2023).

In this study, tephra layers from three cores recovered on the northern shoulder of the Pantelleria Graben to the NE of Pantelleria island, interpreted as primary air-fall deposits, have been analysed with different analytical techniques (EMPA and EDX). Major element compositions of glass shards proved to be effective for confirming their provenance from the nearby Pantelleria and for relating them with the occurrence of explosive events in the recent (post-caldera) history of this volcanic complex. In detail, tephra layers dated as younger than the last ~13.7 ka can be associated with the most recent silicic eruptive cycle recognized at Pantelleria and likely occurred after a volcanic stasis fixed at 12–14 ka ago (Scaillet et al., 2011).

The coarse-grained tephra PAN07-CC, partially sampled in the core catcher at the base of core PAN07, due to its distinctive petrochemical signature and facies has been associated with the Green Tuff eruption (occurred ~45 ka ago). It represents a new near-vent evidence of this important volcanic event, that in the distal marine record is represented by the Y-6 tephra. The relevance of the Y-6 tephra layer as a chronologic and stratigraphic marker in the Mediterranean ("a temporal tie-point" in the paleoclimatic time series, according to Scaillet et al., 2013) is widely recognized. However, the geochemical characterization of this huge explosive event can be biased (i.e., more or less completely recorded) in distal vs. proximal tephra, as it is suggested by the composition of our sample that appears to enlarge the bimodal composition recorded in other distal tephra.

Moreover, the indications provided by this study deserve further research in the marine site we have selected, having a good potential for the record of the Pantelleria eruptive activity. In particular, the possible adoption of more efficient sampling techniques aiming at recovering the sedimentary sequence and whole basal, coarse-grained deposit and better characterizing its inner structure and age, might provide more refined proximal-distal correlations of the GT-related record and of post-GT tephra dispersal pattern, and a more accurate reconstruction of the style and frequency of past eruptive activity of Pantelleria.

Author contributions

Conceptualization: RC, BS, GC; Investigation: RC, GC, GM, BS; Formal analysis and data curation: RC, GC, CAM, GG, GM, CHA, BS, Funding acquisition: BS, RC; Resources: RC, CAM, GG, BS; Supervision: RC; Writing-original draft and visualization: RC, GC, CAM, GG, GM, CHA, BS; Writing-review& editing: RC, GC, CAM, GG, GM, CHA, BS.

Funding

The research has received funding from the European Union Seventh Framework Programme (FP7/2007-2013) under Grant Agreement n° 312762-EUROFLEETS2, project "PANTelleria High-energy ERuptions from marine studies (PANTHER)" (PI S. Benetti). The work was supported by NERC- NEIF Radiocarbon NRCF010001 (allocation number 2017.0418).

CRediT authorship contribution statement

C. Romagnoli: Conceptualization, Data curation, Formal analysis, Funding acquisition, Investigation, Methodology, Resources, Supervision, Writing – original draft, Writing – review & editing. **C. Giglio:** Conceptualization, Data curation, Formal analysis, Investigation, Methodology, Visualization, Writing – original draft. **A.M. Conte:** Data curation, Formal analysis, Methodology, Resources, Writing – original draft, Writing – review & editing. **A. Cloke-Hayes:** Data curation,

Formal analysis, Resources, Writing – original draft, Writing – review & editing. **M. Garcia:** Data curation, Formal analysis, Investigation, Methodology, Writing – original draft. **G. Gasparotto:** Methodology, Data curation, Formal analysis, Resources, Writing – original draft, Writing – review & editing. **S. Benetti:** Conceptualization, Data curation, Formal analysis, Funding acquisition, Investigation, Methodology, Project administration, Resources, Writing – original draft, Writing – review & editing.

Declaration of competing interest

The Authors declare no conflict of interest.

Data availability

Data will be made available on request.

Acknowledgements

We kindly acknowledge the Panther Scientific Party participating to the cruise and the crew of *Minerva Uno*. We are grateful to Alessandro Bosman, Matteo Meli and Elena Scacchia for collaboration. We would also like to thank the School of Geography and Environmental Science at Ulster University for providing additional funding for radiocarbon dating. Lastly, we must acknowledge the significant contribution of our colleague Dr. Aggeliki Georgiopoulou (University College Dublin previously, now at Ternan Energy) to survey design, core sampling, processing and interpretations, and scientific discussions. We also acknowledge two anonymous reviewers for their useful suggestions.

Appendix A. Supplementary data

Supplementary data to this article can be found online at https://doi.org/10.1016/j.jvolgeores.2023.107997.

References

Anastasakis, G., Pe-Piper, G., 2006. An 18 m thick volcaniclastic interval in Pantelleria Trough, Sicily Channel, deposited from a large gravitative flow during the Green Tuff eruption. Mar. Geol. 231, 201–219. https://doi.org/10.1016/j.margeo.2006.06.005.

Astraldi, M., Conversano, F., Civitarese, G., Gasparini, G.P., Ribera d'Alcalà, M., Vetrano, A., 2002. Water mass properties and chemical signatures in the central Mediterranean region. J. Mar. Syst. 33–34, 155–177. https://doi.org/10.1016/S0924-7963(02)00057-X.

Avanzinelli, R., Bindi, L., Menchetti, S., Conticelli, S., 2004. Crystallisation and genesis of peralkaline magmas from Pantelleria Volcano, Italy: an integrated petrological and crystal-chemical study. Lithos 73, 41–69. https://doi.org/10.1016/j.lithos.2003.10.007.

Bosman, A., Calarco, M., Casalbore, D., Conte, A.M., Martorelli, E., Sposato, A., Falese, L., Macelloni, L., Romagnoli, C., Chiocci, F.L., 2011. Volcanic Island: the tips of large submerged volcanoes that only marine geology may reveal (Example from W-Pontine Archipelago, Ischia, Stromboli and Pantelleria). In: Brugnoli, E., Cavaretta, S., Mazzola, S., Trincardi, F., Ravaioli, M., Santoleri, R. (Eds.), Marine Research at CNR, pp. 433–444 volume DTA/06-2011, ISSN 2239-5172.

Burollet, P.F., Muginiot, J.M., Sweeney, P., 1978. The geology of the Pelagian block: the margins and basins of southern Tunisia and Tripolitania. In: Nairn, A.E.M., Kanes, W. H., Stelhi, F.G. (Eds.), The Ocean Basins and Margins: The Western Mediterranean, pp. 331–359. New York.

Calanchi, N., Colantoni, P., Rossi, P.L., Saitta, M., Serri, G., 1989. The Strait of Sicily continental rift systems: physiography and petrochemistry of the submarine volcanic centres. Mar. Geol. 87, 55–83. https://doi.org/10.1016/0025-3227(89)90145-X.

Calanchi, N., Gasparotto, G., Romagnoli, C., 1994. Glass chemistry in volcanoclastic sediments of ODP Leg 107, Site 650, sedimentary sequence: provenance and chronological implications. J. Volcanol. Geotherm. Res. 60, 59–85.

Calanchi, N., Cattaneo, A., Dinelli, E., Gasparotto, G., Lucchini, F., 1998. Tephra layers in Late Quaternary sediments of the central Adriatic Sea. Mar. Geol. 149, 191–209.

Carey, S., 1997. Influence of convective sedimentation on the formation of widespread tephra fall layers in the deep sea. Geology 25 (9), 839–842. https://doi.org/10.1130/0091-7613(1997)025<0839:IOCSOT>2.3.

Caron, B., Sulpizio, R., Zanchetta, G., Siani, G., Santacroce, R., 2010. The late Holocene to Pleistocene tephrostratigraphic record of Lake Ohrid (Albania). Comptes Rendus - Geosci. 342, 453–466. https://doi.org/10.1016/j.crte.2010.03.007.

Caron, B., Siani, G., Sulpizio, R., Zanchetta, G., Paterne, M., Santacroce, R., Tema, E., Zanella, E., 2012. Late Pleistocene to Holocene tephrostratigraphic record from the Northern Ionian Sea. Mar. Geol. 311-314, 41–51.

Cassidy, M., Watt, S.F.L., Palmer, M.R., Trofimovs, J., Symons, W., Maclachlan, S.E., Stinton, A.J., 2014. Construction of volcanic records from marine sediment cores: a review and case study (Montserrat, West Indies). Earth-Sci. Rev. 138, 137–155. https://doi.org/10.1016/j.earscirev.2014.08.008.

Cinquegrani, A., Scaillet, S., Romano, P., Rotolo, S.G., 2022. 40Ar/39Ar dating of the trachytic crystal mush of the Green Tuff ignimbrite, Pantelleria island. In: Conference Paper, September 2022.

Civetta, L., 1998. The geochemistry of volcanic rocks from Pantelleria Island, Sicily Channel: petrogenesis and characteristics of the Mantle Source Region. J. Petrol. 39, 1453–1491. https://doi.org/10.1093/petrology/39.8.1453.

Civetta, L., Cornette, Y., Crisci, G., Gillot, P.Y., Orsi, G., Requejo, C.S., 1984. Geology, geochronology and chemical evolution of the island of Pantelleria. Geol. Mag. 121, 541–562. https://doi.org/10.1017/S0016756800030703.

Civetta, L., Cornette, Y., Gillot, P.Y., Orsi, G., 1988. The eruptive history of Pantelleria (Sicily channel) in the last 50 ka. Bull. Volcanol. 50, 47–57. https://doi.org/10.1007/BF01047508.

Civile, D., Lodolo, E., Accettella, D., Geletti, R., Ben-Avraham, Z., Deponte, M., Facchin, L., Ramella, R., Romeo, R., 2010. The Pantelleria graben (Sicily Channel, Central Mediterranean): an example of intraplate "passive" rift. Tectonophysics 490, 173–183. https://doi.org/10.1016/j.tecto.2010.05.008.

Colantoni, P., 1975. Note di geologia marine sul Canale di Sicilia. G. di Geol. 40, 181–207.

Conte, A.M., Martorelli, E., Calarco, M., Sposato, A., Perinelli, C., Coltelli, M., Chiocci, F. L., 2014. The 1891 submarine eruption offshore Pantelleria Island (Sicily Channel, Italy): identification of the vent and characterization of products and eruptive style. Geochem. Geophys. Geosyst. 2555–2574. https://doi.org/10.1002/2014GC005238.

Cornette, Y., Crisci, G.M., Gillot, P.-Y., Orsi, G., 1983. Recent volcanic history of Pantelleria: a new interpretation. J. Volcanol. Geotherm. Res. 17, 361–373.

Damaschke, M., Sulpizio, R., Zanchetta, G., Wagner, B., Böhm, A., Nowaczyk, N., Rethemeyer, J., Hilgers, A., 2013. Tephrostratigraphic studies on a sediment core from Lake Prespa in the Balkans. Clim. Past 9, 267–287. https://doi.org/10.5194/cp-9-267-2013.

D'Antonio, M., Mariconte, R., Arienzo, I., Mazzeo, F.C., Carandente, A., Perugini, D., Petrelli, M., Corselli, C., Orsi, G., Principato, M.S., Civetta, L., 2016. Combined Sr-Nd isotopic and geochemical fingerprinting as a tool for identifying tephra layers: application to deep-sea cores from Eastern Mediterranean Sea. Chem. Geol. 443, 121–136. https://doi.org/10.1016/j.chemgeo.2016.09.022.

Di Genova, D., Romano, C., Hess, K.U., Vona, A., Poe, B.T., Giordano, D., Dingwell, D.B., Behrens, H., 2013. The rheology of peralkaline rhyolites from Pantelleria Island. J. Volcanol. Geotherm. Res. 249, 201–216. https://doi.org/10.1016/j.jvolgeores.2012.10.017.

Di Roberto, A., Albert, P.G., Colizza, E., Del Carlo, P., Di Vincenzo, G., Gallerani, A., Giglio, F., Kuhn, G., Macrì, P., Manning, C.J., Melis, R., Miserocchi, S., Scateni, B., Smith, V.C., Torricella, F., Winkler, A., 2020. Evidence for a large-magnitude Holocene eruption of Mount Rittmann (Antarctica): a volcanological reconstruction using the marine tephra record. Quat. Sci. Rev. 250, 106629 https://doi.org/10.1016/j.quascirev.2020.106629.

Foerstner, H., 1891. Das Gestein der 1891 bei Pantelleria entstandenen Vulcaninsel und seine Beziehungen zu den Jungsten Eruptivoesteinen der Nachbarschaft. Tsch. Min. Petr. Mitth 12, 510–521.

Förstner, H., 1881. Nota preliminare sulla geologia dell' Isola di Pantelleria secondo gli studi fatti negli anni 1874 e 1881. Boll. R. Com. Geol. It. 12, 523–556.

Freundt, A., Schindlbeck-Belo, J.C., Kutterolf, S., Hopkin, J., 2021. Tephra layers in the marine environment: A review of properties and emplacement processes. In: Di Capua, A., De Rosa, R., Kerszturi, G., Le Pera, E., Rosi, M., Watt, S.F.L. (Eds.), Volcanic Processes in the Sedimentary Record: When Volcenoes Meet the Environment, 520. Geological Society, London, Special Publications, pp. 595–637. https://doi.org/10.1144/SP520-2021-50.

Friedrichs, B., Schindlbeck-Belo, J.C., Danišík, M., Jenkins, S.F., Yurteri, E., Çobankaya, M., Frische, M., Wang, K.L., Lee, H.Y., Atıcı, G., Schmitt, A.K., Sparks, R. S.J., 2020. New insights into source and dispersal of Mediterranean S1 tephra, an early Holocene marker horizon erupted at Mt. Erciyes (Turkey). Quat. Sci. Rev. 249 https://doi.org/10.1016/j.quascirev.2020.106606.

Gasperini, L., Stanghellini, G., 2009. SeisPrho: An interactive computer program for processing and interpretation of high-resolution seismic reflection profiles. Comput. Geosci. 35, 1497–1507. https://doi.org/10.1016/j.cageo.2008.04.014.

Gauchery, T., Rovere, M., Pellegrini, C., Asioli, A., Tesi, T., Cattaneo, A., Trincardi, F., 2021. Post-LGM multi-proxy sedimentary record of bottom-current variability and downslope sedimentary processes in a contourite drift of the Gela Basin (Strait of Sicily). Mar. Geol. 439, 106564. https://doi.org/10.1016/j.margeo.2021.106564.

Giaccio, B., Nomade, S., Wulf, S., Isaia, R., Sottili, G., Cavuoto, G., Galli, P., Messina, P., Sposato, A., Sulpizio, R., Zanchetta, G., 2012. The late MIS 5 Mediterranean tephra markers: a reappraisal from peninsular Italy terrestrial records. Quat. Sci. Rev. 56, 31–45. https://doi.org/10.1016/j.quascirev.2012.09.009.

Giaccio, B., Leicher, N., Mannella, G., Monaco, L., Regattieri, E., Wagner, B., Zanchetta, G., Gaeta, M., Marra, F., Nomade, S., Palladino, D.M., Pereira, A., Scheidt, S., Sottili, G., Wonik, T., Wulf, S., Zeeden, C., Ariztegui, D., Cavinato, G.P., Dean, J.R., Florindo, F., Leng, M.J., Macrì, P., Niespolo, E., Renne, P.R., Rolf, C., Sadori, L., Thomas, C., Tzedakis, P.C., 2019. Extending the tephra and palaeoenvironmental record of the Central Mediterranean back to 430 ka: a new core from Fucino Basin, central Italy. Quat. Sci. Rev. 225 https://doi.org/10.1016/j.quascirev.2019.106003.

Gioncada, A., Landi, P., 2010. The pre-eruptive volatile contents of recent basaltic and pantelleritic magmas at Pantelleria (Italy). J. Volcanol. Geotherm. Res. 189, 191–201. https://doi.org/10.1016/j.jvolgeores.2009.11.006.
Hemleben, C., Spindler, M., Anderson, O.R., 1989. Taxonomy and species features. In: Modern Planktonic Foraminifera. Springer, New York, pp. 8–32.
Hopkins, J.L., Wysoczanski, R.J., Orpin, A.R., Howarth, J.D., Strachan, L.J., Lunenburg, R., McKeown, M., Ganguly, A., Twort, E., Camp, S., 2020. Deposition and preservation of tephra in marine sediments at the active Hikurangi subduction margin. Quat. Sci. Rev. 247, 106500 https://doi.org/10.1016/j.quascirev.2020.106500.
Insinga, D.D., Tamburrino, S., Lirer, F., Vezzoli, L., Barra, M., De Lange, G.J., Tiepolo, M., Vallefuoco, M., Mazzola, S., Sprovieri, M., 2014. Tephrochronology of the astronomically-tuned KC01B deep-sea core, Ionian Sea: insights into the explosive activity of the Central Mediterranean area during the last 200ka. Quat. Sci. Rev. 85, 63–84. https://doi.org/10.1016/j.quascirev.2013.11.019.
Jordan, N.J., Rotolo, S.G., Williams, R., Speranza, F., McIntosh, W.C., Branney, M.J., Scaillet, S., 2018. Explosive eruptive history of Pantelleria, Italy: repeated caldera collapse and ignimbrite for- mation at a peralkaline volcano. J. Volcanol. Geotherm. Res. 349, 47–73. https://doi.org/10.1016/j.jvolgeores.2017.09.013.
Keller, J., Ryan, W.B.F., Ninkovich, D., Altherr, R., 1978. Explosive volcanic activity in the Mediterranean over the past 200,000 yr as recorded in deep-sea sediments. Bull. Geol. Soc. Am. 89, 591–604. https://doi.org/10.1130/0016-7606(1978)89<591:EVAITM>2.0.CO;2.
Kelly, T.J., Carey, S., Pistolesi, M., Rosi, M., CroffBell, K.L.C., Roman, C., Marani, M., 2014. Exploration of the 1891 Foerstner submarine vent site (Pantelleria, Italy): insights into the formation of basaltic balloons. Bull. Volcanol. 76 (844), 1–18. https://doi.org/10.1007/s00445-014-0844-4.
Kuhlmann, J., Asioli, A., Trincardi, F., Klügel, A., Huhn, K., 2015. Sedimentary response to Milankovitch-type climatic oscillations and formation of sediment undulations: evidence from a shallow-shelf setting at Gela Basin on the Sicilian continental margin. Quat. Sci. Rev. 108, 76–94. https://doi.org/10.1016/j.quascirev.2014.10.030.
Lanzo, G., Landi, P., Rotolo, S.G., 2013. Volatiles in pantellerite magmas: a case study of the Green Tuff Plinian eruption (Island of Pantelleria, Italy). J. Volcanol. Geotherm. Res. 262, 153–163. https://doi.org/10.1016/j.jvolgeores.2013.06.011.
Le Bas, M.J., Le Maitre, R.W., Streckeisen, A., Zanettin, B., 1986. A Chemical Classification of Volcanic Rocks Based on the Total Alkali-Silica Diagram. Journal of Petrology 27, 745–750. https://doi.org/10.1093/petrology/27.3.745.
MacDonald, R., 1974. Nomenclature and petrochemistry of the peralkaline oversaturated extrusive rocks. Bull Volcanol 38, 498–516. https://doi.org/10.1007/BF02596896.
Mahood, G.A., Hildreth, W., 1983. Nested calderas and trapdoor uplift at Pantelleria, Strait of Sicily. Geology 11, 103–106.
Mahood, G.A., Hildreth, W., 1986. Geology of the peralkaline volcano at Pantelleria, Strait of Sicily. Bull. Volcanol. 48, 143–172.
Manville, V., Wilson, C.J.N., 2004. The 26.5 ka oruanui eruption, New Zealand: a review of the roles of volcanism and climate in the post-eruptive sedimentary response. New Zeal. J. Geol. Geophys. 47, 525–547. https://doi.org/10.1080/00288306.2004.9515074.
Margari, V., Pyle, D.M., Bryant, C., Gibbard, P.L., 2007. Mediterranean tephra stratigraphy revisited: results from a long terrestrial sequence on Lesvos Island, Greece. J. Volcanol. Geotherm. Res. 163, 34–54. https://doi.org/10.1016/j.jvolgeores.2007.02.002.
Margaritelli, G., Lirer, F., Schroeder, K., Cloke-Hayes, A., Caruso, A., Capotondi, L., Broggy, T., Cacho, I., Sierro, F.J., 2022. Globorotalia truncatulinoides in the Mediterranean Basin during the Middle–Late Holocene: bio-chronological and oceanographic indicator. Geosciences 12 (6), 244. https://doi.org/10.3390/geosciences12060244.
Martorelli, E., Petroni, G., Chiocci, F.L., the Pantelleria Scientific Party, 2011. Contourites offshore Pantelleria Island (Sicily Channel, Mediterranean Sea): depositional, erosional and biogenic elements. Geo-Marine Letters 31, 481–493. https://doi.org/10.1007/s00367-011-0244-0.
Monaco, L., Leicher, N., Palladino, D.M., Arienzo, I., Marra, F., Petrelli, M., Nomade, S., Pereira, A., Sottili, G., Conticelli, S., D'Antonio, M., Fabbrizio, A., Jicha, B.R., Mannella, G., Petrosino, P., Regattieri, E., Tzedakis, P.C.T., Wagner, B., Zanchetta, G., Giaccio, B., 2022. The Fucino 250–170 ka tephra record: new insights on peri-Tyrrhenian explosive volcanism, central mediterranean tephrochronology, and timing of the MIS 8-6 climate variability. Quat. Sci. Rev. 296 https://doi.org/10.1016/j.quascirev.2022.107797. ISSN 0277-3791.
Narcisi, B., Vezzoli, L., 1999. Quaternary stratigraphy of distal tephra layers in the Mediterranean - an overview. Glob. Planet. Change 21, 31–50. https://doi.org/10.1016/S0921-8181(99)00006-5.
Orsi, G., Sheridan, M.F., 1984. The Green Tuff of Pantelleria: Rheoignimbrite or rheomorphic fall? Bull. Volcanol. 47, 611–626. https://doi.org/10.1007/BF01961230.
Orsi, G., Ruvo, L., Scarpati, C., 1991. The recent explosive volcanism at Pantelleria. Geol. Rundsch. 80, 187–200. https://doi.org/10.1007/BF01828776.
Paterne, M., Guichard, F., Labeyrie, J., Gillot, P.Y., Duplessy, J.C., 1986. Tyrrhenian Sea tephrochronology of the oxygen isotope record for the past 60,000 years. Mar. Geol. 72 (259), 285.
Paterne, M., Guichard, F., Labeyrie, J., 1988. Explosive activity of the South Italian volcanoes during the past 80,000 years as determined by marine tephrochronology. J. Volcanol. Geotherm. Res. 34, 153–172. https://doi.org/10.1016/0377-0273(88)90030-3.
Paterne, M., Guichard, F., Duplessy, J.C., Siani, G., Sulpizio, R., Labeyrie, J., 2008. A 90,000-200,000 yrs marine tephra record of Italian volcanic activity in the Central Mediterranean Sea. J. Volcanol. Geotherm. Res. 177, 187–196. https://doi.org/10.1016/j.jvolgeores.2007.11.028.
Pizer, C.O., Howarth, J.D., Clark, K.J., Wilson, C.J.N., Tickle, S.E., Hopkins, J.L., Dahl, J. A., 2023. An integrated proximal-distal radiocarbon dating approach provides improved age constraints for key Holocene tephra isochron. Quat. Sci. Rev. 307, 108069. ISSN 0277-3791. https://doi.org/10.1016/j.quascirev.2023.108069.
Pouchou, J.L., Pichoir, F., 1991. Quantitative analysis of homogeneous or stratified microvolumes applying the model "PAP,". In: Heinrich, K.F.J., Newbury, D.E. (Eds.), Electron Probe Quantification. Plenum Press, New York, pp. 31–75.
Riccò, A., 1892. Terremoti, sollevamento ed eruzione sottomarina a Pantelleria nella seconda metà dell'ottobre 1891. In: Annali dell'Ufficio Centr. Meteorol. e Geodinamico Ital. Ser. IIa, Pt. 3, vol. XI, 7-27, Roma.
Rohling, E.J., Jorissen, F.J., Vergnaud Grazzini, C., Zachariasse, W.J., 1993. Northern Levantine and Adriatic Quaternary planktic foraminifera; reconstruction of paleoenvironmental gradients. Mar. Micropaleontol. 21, 191–218.
Rotolo, S.G., Scaillet, S., La Felice, S., Vita-Scaillet, G., 2013. A revision of the structure and stratigraphy of pre-Green Tuff ignimbrites at Pantelleria (Strait of Sicily). J. Volcanol. Geotherm. Res. 250, 61–74. https://doi.org/10.1016/j.jvolgeores.2012.10.009.
Rotolo, S.G., Scaillet, S., Speranza, F., White, J.C., Williams, R., Jordan, N.J., 2021. Volcanological evolution of Pantelleria Island (Strait of Sicily) peralkaline volcano: a review. Comptes Rendus - Geosci. 353, 1–22. https://doi.org/10.5802/CRGEOS.51.
Scaillet, S., Rotolo, S.G., La Felice, S., Vita-Scaillet, G., 2011. High-resolution 40Ar/39Ar chronostratigraphy of the post-caldera (<20ka) volcanic activity at Pantelleria, Sicily Strait. Earth Planet. Sci. Lett. 309 (3–4), 280–290. https://doi.org/10.1016/j.epsl.2011.07.009.
Scaillet, S., Vita-Scaillet, G., Rotolo, S.G., 2013. Millennial-scale phase relationships between ice-core and Mediterranean marine records: insights from high-precision 40Ar/39Ar dating of the Green Tuff of Pantelleria, Sicily Strait. Quat. Sci. Rev. 78, 141–154. https://doi.org/10.1016/j.quascirev.2013.08.008.
Speranza, F., Di Chiara, A., Rotolo, S.G., 2012. Correlation of welded ignimbrites on Pantelleria (Strait of Sicily) using paleomagnetism. Bull. Volcanol. 74, 341–357. https://doi.org/10.1007/s00445-011-0521-9.
Speranza, F., Landi, P., D'Ajello Caracciolo, F., Pignatelli, A., 2010. Paleomagnetic dating of the most recent silicic eruptive activity at Pantelleria (Strait of Sicily). Bull Volcanol 72, 847–858. https://doi.org/10.1007/s00445-010-0368-5.
Sprovieri, R., Di Stefano, E., Incarbona, A., Gargano, M.E., 2003. A high-resolution record of the last deglaciation in the Sicily Channel based on foraminifera and calcareous nannofossil quantitative distribution. Palaeogeogr. Palaeoclimatol. Palaeoecol. 202, 119–142. https://doi.org/10.1016/S0031-0182(03)00632-1.
Stow, D.A.V., Piper, D.J.W., 1984. Deep-water fine-grained sediments: Facies models. In: Stow, D.A.V., Piper, D.J.W. (Eds.), Fine-Grained Sediments: Deep-Water Processes and Facies. Geological Society of London Special Publication 15. Blackwell Scientific Publications, Oxford, pp. 611–645.
Stuiver, M., Reimer, P.J., Reimer, R.W., 2021. CALIB 8.20. http://calib.org/ accessed 2021-7-1.
Sulpizio, R., Bonasia, R., Dellino, P., Di Vito, M.A., La Volpe, L., Mele, D., Zanchetta, G., Sadori, L., 2008. Discriminating the long distance dispersal of fine ash from sustained columns or near ground ash clouds: the example of the Pomici di Avellino eruption (Somma-Vesuvius, Italy). J. Volcanol. Geotherm. Res. 177, 263–276. https://doi.org/10.1016/j.jvolgeores.2007.11.012.
Sulpizio, R., Van Welden, A., Caron, B., Zanchetta, G., 2010. The Holocene tephrostratigraphic record of Lake Shkodra (Albania and Montenegro). J. Quat. Sci. 25, 633–650. https://doi.org/10.1002/jqs.1334.
Tamburrino, S., 2008. Ph.D. Thesis Mediterranean Tephrochronology: New Insights from High-Resolution Analyses of a 200,000 years long Composite Sedimentary Record. Università degli Studi di Napoli "Federico II", 152 pp.
Tamburrino, S., Insinga, D.D., Sprovieri, M., Petrosino, P., Tiepolo, M., 2012. Major and trace element characterization of tephra layers offshore Pantelleria Island: Insights into the last 200 ka of volcanic activity and contribution to the Mediterranean tephrochronology. J. Quat. Sci. 27, 129–140. https://doi.org/10.1002/jqs.1504.
Tamburrino, S., Insinga, D.D., Pelosi, N., Kissel, C., Laj, C., Capotondi, L., Sprovieri, M., 2016. Tephrochronology of a ~ 70 ka-long marine record in the Marsili Basin (southern Tyrrhenian Sea). J. Volcanol. Geotherm. Res. 327, 23–39. https://doi.org/10.1016/j.jvolgeores.2016.07.002.
Tomlinson, E.L., Smith, V.C., Albert, P.G., Aydar, E., Civetta, L., Cioni, R., Çubukçu, E., Gertisser, R., Isaia, R., Menzies, M.A., Orsi, G., Rosi, M., Zanchetta, G., 2015. The major and trace element glass compositions of the productive Mediterranean volcanic sources: tools for correlating distal tephra layers in and around Europe. Quat. Sci. Rev. 118, 48–66. https://doi.org/10.1016/j.quascirev.2014.10.028.
Totaro, F., Insinga, D.D., Lirer, F., Margaritelli, G., Català i Caparrós, A., de la Fuente, M., Petrosino, P., 2022. The Late Pleistocene to Holocene tephra record of ND14Q site (southern Adriatic Sea): traceability and preservation of Neapolitan explosive products in the marine realm. J. Volcanol. Geotherm. Res. 423, 107461.
Vakhrameeva, P., Koutsodendris, A., Wulf, S., Portnyagin, M., Appelt, O., Ludwig, T., Trieloff, M., Pross, J., 2021. Land-sea correlations in the Eastern Mediterranean region over the past c. 800 kyr based on macro- and cryptotephras from ODP Site 964 (Ionian Basin). Quat. Sci. Rev. 255 https://doi.org/10.1016/j.quascirev.2021.106811.
Villari, L., 1974. The island of Pantelleria. Bull. Volcanol. 38, 680–724. https://doi.org/10.1007/BF02596904.
Vogel, H., Zanchetta, G., Sulpizio, R., Wagner, B., Nowaczyk, N., 2010. A tephrostratigraphic record for the last glacial–interglacial cycle from Lake Ohrid, Albania and Macedonia. J. Quat. Sci. 25, 320–338. https://doi.org/10.1002/jqs.
Washington, H.S., 1909. The submarine eruption of 1831 and 1891 near Pantelleria. Am. J. Sci. 27, 131–150.

White, J.C., Parker, D.F., Ren, M., 2009. The origin of trachyte and pantellerite from Pantelleria, Italy: insights from major element, trace element, and thermodynamic modelling. J. Volcanol. Geotherm. Res. 179, 33–55. https://doi.org/10.1016/j.jvolgeores.2008.10.007.

Williams, R., 2010. Emplacement of Radial Pyroclastic Density Currents over Irregular Topography: The Chemically-Zoned, Low Aspect-Ratio Green Tuff Ignimbrite. PhD thesis,. University of Leicester, Pantelleria, Italy. https://doi.org/10.6084/m9.figshare. 789054.v1.

Wolff, J.A., Wright, J.V., 1981. Formation of the Green Tuff, Pantelleria. Bull. Volcanol. 44, 681–690.

Wulf, S., Hardiman, M.J., Staff, R.A, Koutsodendris, A., Appelt, O., Blockley, S.P.E., Lowe, J.J., Manning, C.J., Ottolini, L., Schmitt, A.K., Smith, V.C., Tomlinson, E.L., Vakhrameeva, P., Knipping, M., Kotthoff, U., Milner, A.M., Müller, U.C., Christanis, K., Kalaitzidis, S., Tzedakis, P.C., Schmiedl, G., Pross, J., 2018. The marine isotope stage 1–5 cryptotephra record of Tenaghi Philippon, Greece: towards a detailed tephrostratigraphic framework for the Eastern Mediterranean region. Quat. Sci. Rev. 186, 236–262. https://doi.org/10.1016/j.quascirev.2018.03.011.

Wuthke, K., Wulf, S., Tomlinson, E.L., Hardiman, M., Dulski, P., Luterbacher, J., Brauer, A., 2016. Geochemical properties and environmental impacts of seven Campanian tephra layers deposited between 40 and 38 ka BP in the varved lake sediments of Lago Grande di Monticchio, southern Italy. Quat. Sci. Rev. 118, 67–83. https://doi.org/10.1016/j.quascirev.2014.05.017.

Zanchetta, G., Giaccio, B., Bini, M., Sarti, L., 2018. Tephrostratigraphy of Grotta del Cavallo, Southern Italy: Insights on the chronology of Middle to Upper Palaeolithic transition in the Mediterranean. Quat. Sci. Rev. 182, 65–77. https://doi.org/10.1016/j.quascirev.2017.12.014.